AFRL-AFOSR-UK-TR-2021-0009

Hypersonic Intake Testing with Varying Wall Temperature

McGilvray, Matthew
THE UNIVERSITY OF OXFORD
UNIVERSITY OFFICES
OXFORD, ,
GB

04/30/2021
Final Technical Report

Air Force Research Laboratory
Air Force Office of Scientific Research
European Office of Aerospace Research and Development
Unit 4515 Box 14, APO AE 09421

REPORT DOCUMENTATION PAGE

Form Approved
OMB No. 0704-0188

1. REPORT DATE *(DD-MM-YYYY)*	**2. REPORT TYPE**	**3. DATES COVERED** *(From - To)*
30-04-2021	Final	15 Oct 2017 - 14 Oct 2020

4. TITLE AND SUBTITLE
Hypersonic Intake Testing with Varying Wall Temperature

5a. CONTRACT NUMBER

5b. GRANT NUMBER
FA9550-18-1-0022

5c. PROGRAM ELEMENT NUMBER
61102F

6. AUTHOR(S)
Matthew McGilvray

5d. PROJECT NUMBER

5e. TASK NUMBER

5f. WORK UNIT NUMBER

7. PERFORMING ORGANIZATION NAME(S) AND ADDRESS(ES)
THE UNIVERSITY OF OXFORD
UNIVERSITY OFFICES
OXFORD,
GB

8. PERFORMING ORGANIZATION REPORT NUMBER

9. SPONSORING/MONITORING AGENCY NAME(S) AND ADDRESS(ES)
EOARD
UNIT 4515
APO AE 09421-4515

10. SPONSOR/MONITOR'S ACRONYM(S)
AFRL/AFOSR IOE

11. SPONSOR/MONITOR'S REPORT NUMBER(S)
AFRL-AFOSR-UK-TR-2021-0009

12. DISTRIBUTION/AVAILABILITY STATEMENT
A Distribution Unlimited: PB Public Release

13. SUPPLEMENTARY NOTES

14. ABSTRACT
This project set out to experimentally characterise a three-dimensional shape transition scramjet intake at off-design, low Mach number (M = 5) test conditions. The intake of interest was a Conical-Rectangular-to-Elliptical-Shape-Transition (C-REST) intake developed by Dr Rowan Gollan and Prof. Michael Smart of the University of Queensland (Gollan and Smart, 2013) for the three-stage access-to-space vehicle SPARTAN (Preller and Smart, 2017). It had a design point of Mach 10 and was required to operate down to at least Mach 5. Although the C-REST intake was an evolution of the earlier REST methodologies of Smart (1999), prior to this project the mass capture, back-pressure and self-starting capabilities of this class of intake had not been characterised. Such a characterisation is typically undertaken experimentally in relatively long-duration hypersonic facilities such as the Oxford High Density Tunnel (HDT). Initially a one-year project which coincided with Prof. Smart's sabbatical visit to the University of Oxford, this project was extended to three years to allow development of a novel mass capture device known as MassCap.

15. SUBJECT TERMS

16. SECURITY CLASSIFICATION OF:			**17. LIMITATION OF ABSTRACT**	**18. NUMBER OF PAGES**	**19a. NAME OF RESPONSIBLE PERSON**
a. REPORT	**b. ABSTRACT**	**c. THIS PAGE**			DOUGLAS SMITH
U	U	U	SAR	28	**19b. TELEPHONE NUMBER** *(Include area code)* 314 235 6013

REPORT DOCUMENTATION PAGE

Form Approved
OMB No. 0704-0188

PLEASE DO NOT RETURN YOUR FORM TO THE ABOVE ADDRESS.

1. REPORT DATE *(DD-MM-YYYY)*	2. REPORT TYPE	3. DATES COVERED *(From - To)*
29-04-2021	Final	Oct 2017 - Oct 2020

4. TITLE AND SUBTITLE

Hypersonic Intake Testing with Varying Wall Temperature

5a. CONTRACT NUMBER

5b. GRANT NUMBER

FA9550-18-1-0022

5c. PROGRAM ELEMENT NUMBER

61102F

6. AUTHOR(S)

Luke Doherty and Matthew McGilvray

5d. PROJECT NUMBER

5e. TASK NUMBER

5f. WORK UNIT NUMBER

7. PERFORMING ORGANIZATION NAME(S) AND ADDRESS(ES)

UNIVERSITY OF OXFORD
WELLINGTON SQUARE
OXFORD OX1 2JD UK

8. PERFORMING ORGANIZATION REPORT NUMBER

9. SPONSORING/MONITORING AGENCY NAME(S) AND ADDRESS(ES)

AFOSR/IOE
86 Blenheim Crescent
Ruislip
HA4 7HB
UK

10. SPONSOR/MONITOR'S ACRONYM(S)

AFOSR/IOE

11. SPONSOR/MONITOR'S REPORT NUMBER(S)

12. DISTRIBUTION/AVAILABILITY STATEMENT

Distribution Statement A: Approved for public release; distribution is unlimited.

13. SUPPLEMENTARY NOTES

14. ABSTRACT

This project set out to experimentally characterise a three-dimensional shape transition scramjet intake at off-design, low Mach number (M = 5) test conditions. The intake of interest was a Conical-Rectangular-to-Elliptical-Shape-Transition (C-REST) intake developed by Dr Rowan Gollan and Prof. Michael Smart of the University of Queensland (Gollan and Smart, 2013) for the three-stage access-to-space vehicle SPARTAN (Preller and Smart, 2017). It had a design point of Mach 10 and was required to operate down to at least Mach 5. Although the C-REST intake was an evolution of the earlier REST methodologies of Smart (1999), prior to this project the mass capture, back-pressure and self-starting capabilities of this class of intake had not been characterised. Such a characterisation is typically undertaken experimentally in relatively long-duration hypersonic facilities such as the Oxford High Density Tunnel (HDT). Initially a one-year project which coincided with Prof. Smart's sabbatical visit to the University of Oxford, this project was extended to three years to allow development of a novel mass capture device known as MassCap.

15. SUBJECT TERMS

hypersonic, scramjet, inlet

16. SECURITY CLASSIFICATION OF:			17. LIMITATION OF ABSTRACT	18. NUMBER OF PAGES	19a. NAME OF RESPONSIBLE PERSON
a. REPORT	b. ABSTRACT	c. THIS PAGE			19b. TELEPHONE NUMBER *(Include area code)*
U	U	U	UU		

Reset

Standard Form 298 (Rev. 8/98)
Prescribed by ANSI Std. Z39.18

INSTRUCTIONS FOR COMPLETING SF 298

1. REPORT DATE. Full publication date, including day, month, if available. Must cite at least the year and be Year 2000 compliant, e.g. 30-06-1998; xx-06-1998; xx-xx-1998.

2. REPORT TYPE. State the type of report, such as final, technical, interim, memorandum, master's thesis, progress, quarterly, research, special, group study, etc.

3. DATES COVERED. Indicate the time during which the work was performed and the report was written, e.g., Jun 1997 - Jun 1998; 1-10 Jun 1996; May - Nov 1998; Nov 1998.

4. TITLE. Enter title and subtitle with volume number and part number, if applicable. On classified documents, enter the title classification in parentheses.

5a. CONTRACT NUMBER. Enter all contract numbers as they appear in the report, e.g. F33615-86-C-5169.

5b. GRANT NUMBER. Enter all grant numbers as they appear in the report, e.g. AFOSR-82-1234.

5c. PROGRAM ELEMENT NUMBER. Enter all program element numbers as they appear in the report, e.g. 61101A.

5d. PROJECT NUMBER. Enter all project numbers as they appear in the report, e.g. 1F665702D1257; ILIR.

5e. TASK NUMBER. Enter all task numbers as they appear in the report, e.g. 05; RF0330201; T4112.

5f. WORK UNIT NUMBER. Enter all work unit numbers as they appear in the report, e.g. 001; AFAPL30480105.

6. AUTHOR(S). Enter name(s) of person(s) responsible for writing the report, performing the research, or credited with the content of the report. The form of entry is the last name, first name, middle initial, and additional qualifiers separated by commas, e.g. Smith, Richard, J, Jr.

7. PERFORMING ORGANIZATION NAME(S) AND ADDRESS(ES). Self-explanatory.

8. PERFORMING ORGANIZATION REPORT NUMBER. Enter all unique alphanumeric report numbers assigned by the performing organization, e.g. BRL-1234; AFWL-TR-85-4017-Vol-21-PT-2.

9. SPONSORING/MONITORING AGENCY NAME(S) AND ADDRESS(ES). Enter the name and address of the organization(s) financially responsible for and monitoring the work.

10. SPONSOR/MONITOR'S ACRONYM(S). Enter, if available, e.g. BRL, ARDEC, NADC.

11. SPONSOR/MONITOR'S REPORT NUMBER(S). Enter report number as assigned by the sponsoring/ monitoring agency, if available, e.g. BRL-TR-829; -215.

12. DISTRIBUTION/AVAILABILITY STATEMENT. Use agency-mandated availability statements to indicate the public availability or distribution limitations of the report. If additional limitations/ restrictions or special markings are indicated, follow agency authorization procedures, e.g. RD/FRD, PROPIN, ITAR, etc. Include copyright information.

13. SUPPLEMENTARY NOTES. Enter information not included elsewhere such as: prepared in cooperation with; translation of; report supersedes; old edition number, etc.

14. ABSTRACT. A brief (approximately 200 words) factual summary of the most significant information.

15. SUBJECT TERMS. Key words or phrases identifying major concepts in the report.

16. SECURITY CLASSIFICATION. Enter security classification in accordance with security classification regulations, e.g. U, C, S, etc. If this form contains classified information, stamp classification level on the top and bottom of this page.

17. LIMITATION OF ABSTRACT. This block must be completed to assign a distribution limitation to the abstract. Enter UU (Unclassified Unlimited) or SAR (Same as Report). An entry in this block is necessary if the abstract is to be limited.

EOARD SPARTAN INTAKE TESTING: Final Report

Luke Doherty, Chris Hambidge, Matthew McGilvray and Michael Smart

Project Title: Hypersonic Intake Testing with Varying Wall Temperature

Award Number: FA9550-18-1-0022

Objective: To perform aerodynamic testing of the SPARTAN CREST scramjet intake at the lower end of its operational envelope in the Oxford High Density Tunnel to determine the

1. Inlet efficiency and boundary-layer transition location;
2. Self-starting limit;
3. Mass capture and back-pressure limit.

Additionally, a novel back pressure device that allows for independent and accurate measurement of the mass flow rate is to be developed. This device is to be verified with the testing of a 100% capture Pitot Intake.

1. Project Summary: This project set out to experimentally characterise a three-dimensional shape transition scramjet intake at off-design, low Mach number (M = 5) test conditions. The intake of interest was a Conical-Rectangular-to-Elliptical-Shape-Transition (C-REST) intake developed by Dr Rowan Gollan and Prof. Michael Smart of the University of Queensland (Gollan and Smart, 2013) for the three-stage access-to-space vehicle SPARTAN (Preller and Smart, 2017). It had a design point of Mach 10 and was required to operate down to at least Mach 5. Although the C-REST intake was an evolution of the earlier REST methodologies of Smart (1999), prior to this project the mass capture, back-pressure and self-starting capabilities of this class of intake had not been characterised. Such a characterisation is typically undertaken experimentally in relatively long-duration hypersonic facilities such as the Oxford High Density Tunnel (HDT).

Initially a one-year project which coincided with Prof. Smart's sabbatical visit to the University of Oxford, this project was extended to three years to allow development of a novel mass capture device known as MassCap. Three test campaigns were completed in the Oxford High Density Tunnel (HDT) over the period of 2019 through 2020, totalling 33 days of testing (and trouble-shooting/setup) and 88 shots. This report provides a summary of the project and is arranged as follows – Section 2 presents the experimental capabilities that were developed as a part of this project, beginning with the mass capture device MassCap, and continuing with descriptions of the total temperature probe, model attitude probe and ISO 15377 bench-top mass flow calibration rig. Section 2 finishes with descriptions of the three intakes tested, two 100% capture Pitot intakes and the C-REST intake that was of primary interest. Section 3 then provides brief summaries of each test campaign, highlighting the major accomplishments and difficulties encountered in each before the report concludes in Section 3 with an outlook to future work.

2. Capability and Experimental Models Developed

This section summarises the capability and/or models that have been developed over the course of this project.

2.1 Mass Capture Device (MassCap)

The primary outcome of this project has been the development and evaluation of a novel mass flow measurement device called MassCap, where the mass flow measurement and back-pressure capabilities are separate functions. Shown schematically in Figure 1 MassCap consists of a dump-isolator downstream of the high-speed inlet and a secondary isolator downstream of a variable area restrictor. Through appropriate selection of the area ratios of the combined device-intake system, the variable flow path restrictor can be used to set the intake back pressure. The subsequent subsonic flow downstream of the restrictor is reaccelerated through a fixed area, choked measurement nozzle. The inclusion of a calibrated nozzle minimises uncertainties in the mass flow measurement, enhancing the overall accuracy of the device. An isometric exploded view of the complete MassCap assembly is provided in Figure 2.

The variable area restrictor consists of two perforated, circular plates that rotate relative to each other in a controlled manner as shown in Figure 3 and Figure 4. The upstream plate is held fixed while the downstream plate is rotated by a stepper motor that is housed outside the main flow path. Since the plate is driven perpendicular to the flow, the motor experiences less load than the translating cone devices that are typically use for mass flow measurement in short duration facilities. Consequently, rapid controlled changes in restriction area are possible, potentially allowing the mass capture characteristics during a complete start-unstart event of an inlet to be measured transiently in a single experiment. Furthermore, the hole patterns may be specified so as to optimise the back-pressure profile relative to the actuation. The simple annular slots seen in Figure 3 were used exclusively in this project. A photograph of the partially assembled MassCap showing the perforated plates and drive motor is given in Figure 4.

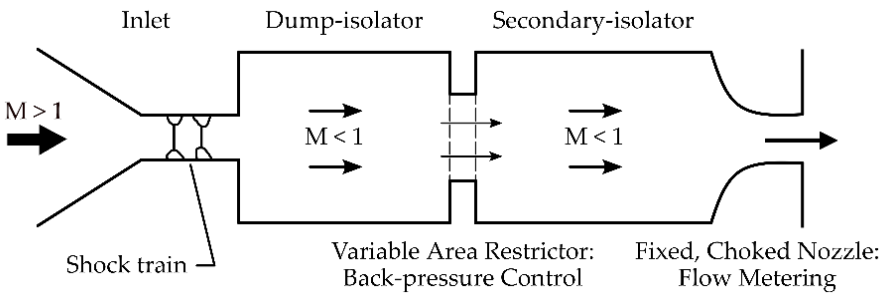

Figure 1: Schematic of novel mass flow measurement / back pressure device

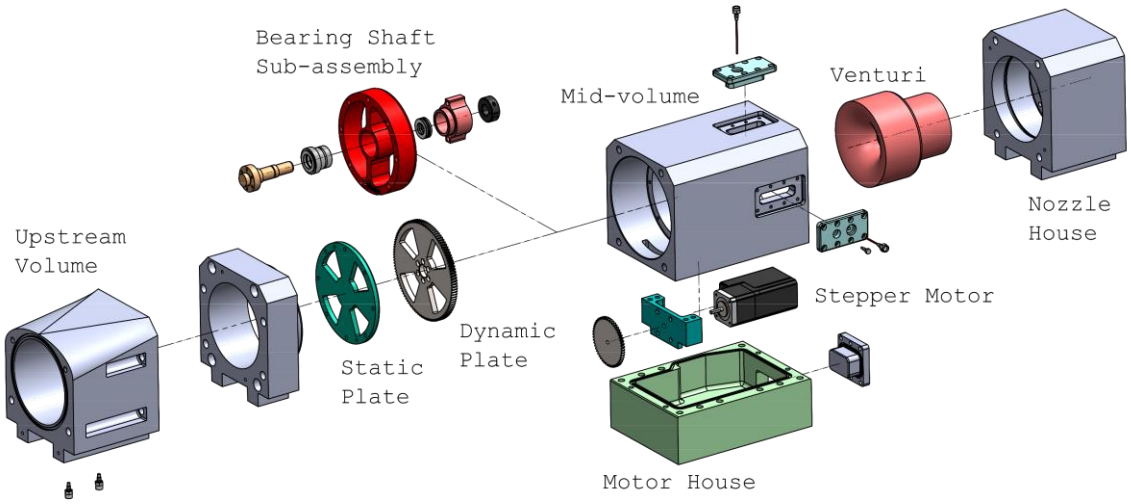

Figure 2: Isometric exploded view of MassCap

MassCap was machined from 7075-T6 billet aluminium and has a maximum pressure rating of 35 bar. The bore is 120 mm and the overall length is 410 mm. The nominal venturi has an exit diameter of 40 mm and was designed in accordance with ISO 9300:2005(E). A second venturi with an exit diameter of 60 mm was also designed and used in the first test campaign with Pitot Intake A (see Sections 2.5 and 3.1). The back-pressure device was located 204 mm downstream of the entrance to MassCap.

In its final form (Campaign 3), MassCap was instrumented with five absolute pressure transducers and four thermocouples as identified in Figure 5. P_{MC1}, P_{MC2} and T_{MC1} are located upstream of the variable area restrictor, P_{MC3}, P_{MC3A}, T_{MC2}, T_{MC2A} and T_{MC2B} were located upstream of the venturi and P_{MC4} was located at the exit of MassCap on the backward facing step. P_{MC3A} was a Kulite XTL-140-100A transducer with range 0 to 100 psi while the other pressure sensors were Kulite XT-190(S)M with range 0 to 3500 kPa. TMC1 and TMC2 were each 0.005 inch diameter K-type thermocouples with the bead positioned approximately 1 mm proud of the internal surface. T_{MC2A} and T_{MC2B} were each 0.003 inch diameter K-type thermocouples with the beads positioned approximately 45 mm and 60 mm proud of the internal surface. P_{MC3A}, T_{MC2A} and T_{MC2B} were each added after the second test campaign to improve our measurement of the pressure and temperature upstream of the venturi, decreasing the overall uncertainty and increasing the system redundancy. These sensors were mounted in access ports in the side and top of MassCap.

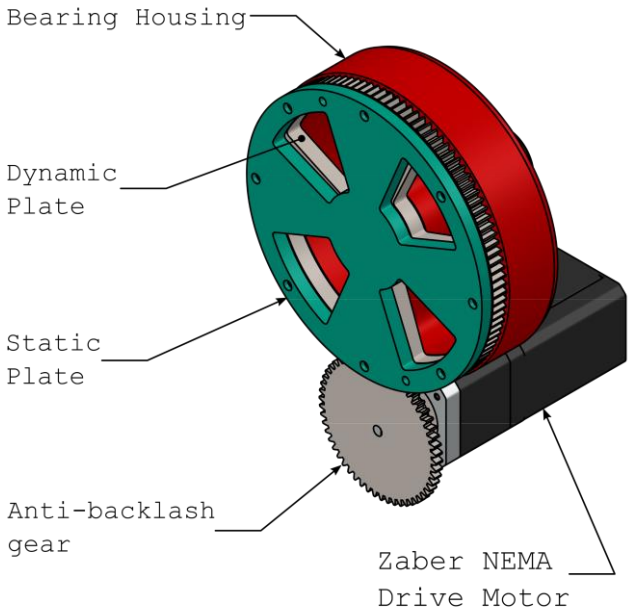

Figure 3: Isometric view of Back Pressure Device Assembly

Dynamic movement of the back-pressure device was developed by a visiting University of Queensland master's student, Syed Zaid Nizami as a part of his industry placement at Oxford (Nizami, 2020). The final system consisted of an Arduino Uno R3 micro-controller board used in conjunction with a Zaber X-Series Shield. The Zaber X-series shield converted the I2C protocol signals generated by the Arduino to the RS-232 signals required by the Zaber motor. A simple Arduino script was used to control the motor in terms of desired rotation angle and speed and the system could be triggered by an input TTL pulse generated by the HDT facility control system. A number of technical challenges were encountered during the development of this capability including:

- Achieving reliable and consistent homing of the dynamic plate/motor
- Slippage of the dynamic plate with respect to the motor shaft at large accelerations
- Execution speed of Arduino script
- Thermal over-heating of the motor when operated in the vacuum environment of the HDT test section
- Overshoot of the dynamic plate (with respect to the commanded final position) due to inertia of the dynamic plate and interfacing gear
- Unknown and currently unquantified delay between the Arduino and Zaber motor (i.e. the delay between sending a command and it being executed)

The first three issues were solved during the third campaign, the overheating of the motor was managed during testing while the final two issues require further work to address, including modifying MassCap to feature an independent position sensor for the dynamic plate. Further work is required to achieve the goal of dynamic, rapid control of the back-pressure device.

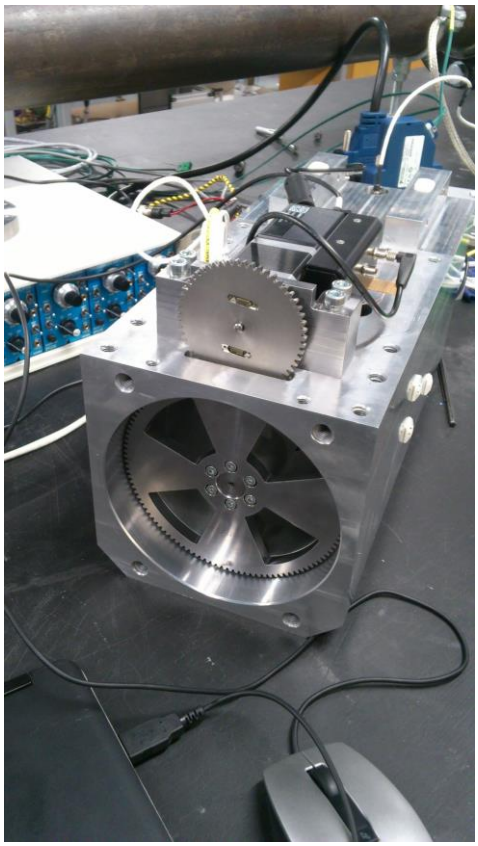

Figure 4: Partially assembled MassCap showing the back-pressure device (slotted plates and associated drive motor).

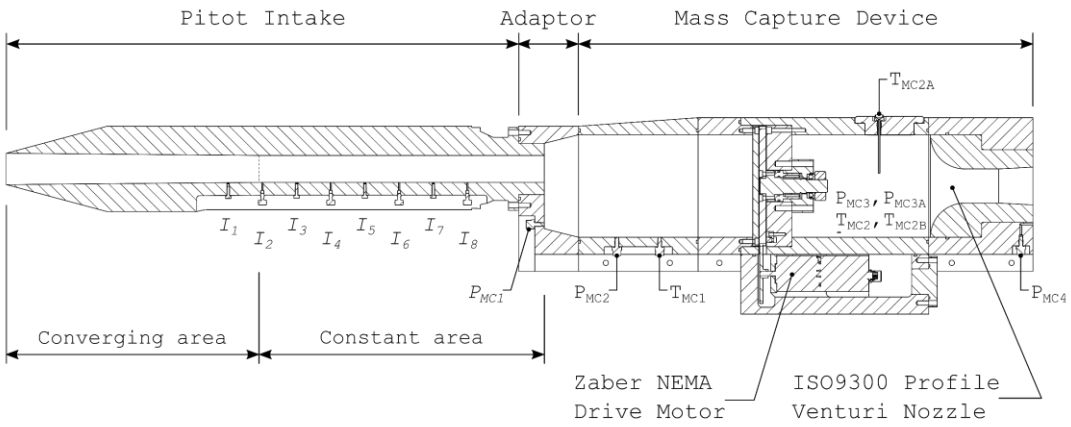

Figure 5: Cross-section through the mid-plane of the MassCap and Pitot Intake B assembly. For clarity, the associated mounting hardware is not shown.

2.2 Total Temperature Probe

To enable accurate transient measurement of the HDT nozzle exit flow condition during each test, a total temperature probe and twin-probe mounting were designed as shown in Figure 6 and Figure 7. Each total temperature probe consisted of an aspirated thermocouple (ATC) housed within a 10.5 mm diameter housing and featuring a 1.6 mm diameter through hole.

The operational principles of the probe are based on heat transfer to a cylinder in a subsonic cross-flow, where the subsonic flow is created by the bow shock that forms in front of the probe and a central hole through the probe provides a suitable gas path, enabling a cross-flow to be established over a suspended thermocouple (TC). The design shown in Figure 6 is essentially a miniaturised version of that developed by Hermann et al. (2019) whose work was in-turn based on that of Widodo and Buttsworth (2013). The twin probe mounting system evolved from the requirement that the gas passing over the thermocouple must exit the rear of the probe.

In the current work, the twin probe mount was instrumented with two ATCs, one with nominal diameter 0.001 inch (1 thou), the other with nominal diameter 0.005 inch (5 thou). Both were K-type thermocouples. These were chosen as prior testing by Hermann et al. (2019) indicated that the faster response of the 1 thou TC was beneficial for analysis however it was less robust than the 5 thou under the aerodynamic loading, particularly at HDT fill pressures >~20 bar.

The small size of the aspirated thermocouple probe was necessary to ensure it could be positioned within the core flow alongside the MassCap and inlet (either Pitot or CREST) assembly during testing and not lead to unwanted flow interactions with the inlet capture stream-tube. Figure 8 shows a photograph of the twin-probe rake installed in the HDT test section along with the Pitot Intake as a part of the current work. The twin-probe mounting and aspirated thermocouples have since been used by multiple other experimental campaigns, including three UK DSTL sponsored programs (Figure 9) and nozzle characterisation work (Figure 10).

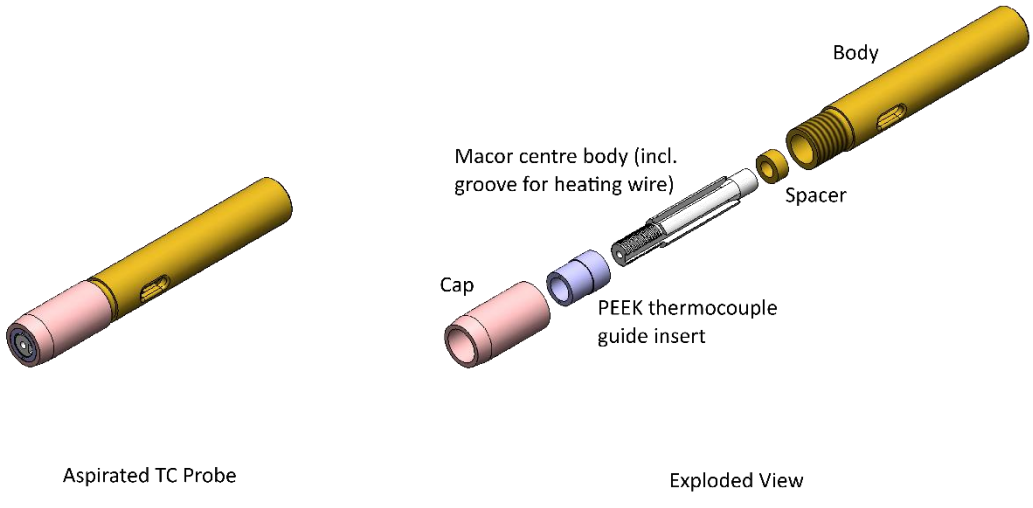

Figure 6: Aspirated Thermocouple Probe (CAD image)

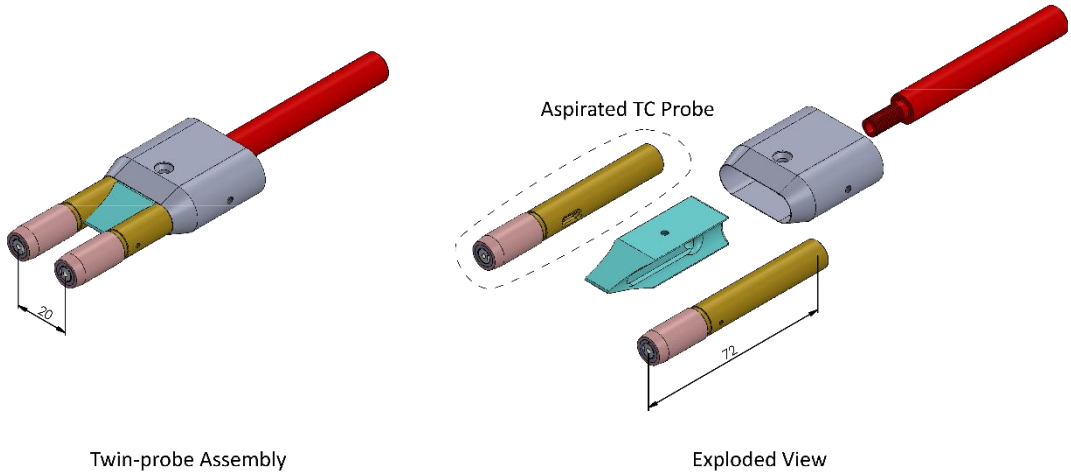

Figure 7: Twin-probe Mount instrumented with Aspirated Thermocouple Probes (CAD Image)

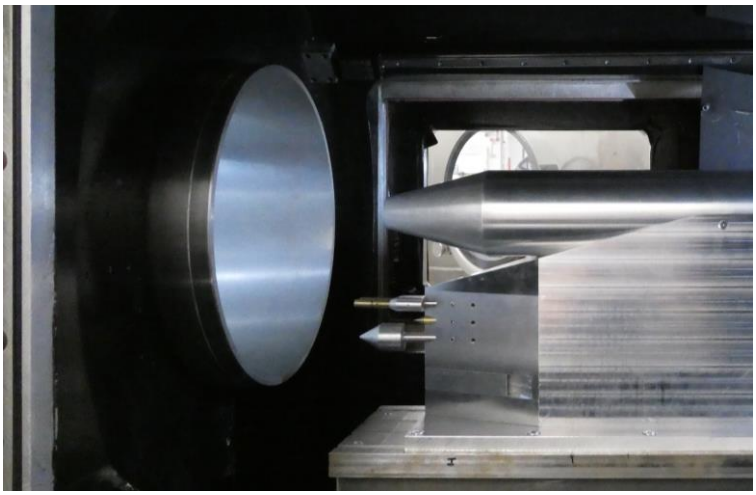

Figure 8: Twin-probe and Model Alignment Probe in-use for the current work.

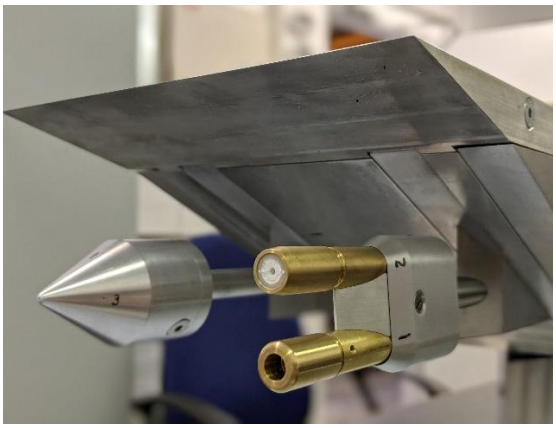

Figure 9: Twin-probe (on the right), with one probe un-instrumented and Model Alignment Probe (on the left) installed on a DSTL-sponsored flat-plate model.

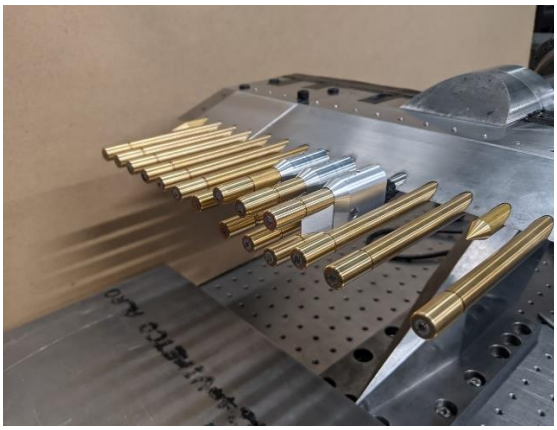

Figure 10: Nozzle survey rake instrumented with twin-probe mounts. Each twin-probe mount features a single aspirated thermocouple and Pitot pressure probe (circa-2021).

2.3 Model Alignment Probe

Shown in Figure 8 and Figure 9 is the Model Alignment Probe (MAP) that was developed for this project by Bustard (2019)[1] to permit an assessment of the alignment (in pitch and yaw) of the intake with respect to the facility nozzle exit flow. The probe consists of a 30-degree half angle blunted cone with nose radius 1.5 mm. The probe is in essence a 5-hole probe, featuring four pressure taps on the conical face for the measurement of pitch and yaw alignment, and one pressure tap at the nose stagnation point for the measurement of Pitot pressure. The probe was instrumented with four Kulite XCEL-152 pressure sensors with range 170 kPa absolute and one Kulite XTL-140 sensor with range 350 kPa absolute.

Prior to its use in the current work, MAP was evaluated by testing it in the High Density Tunnel with the Mach 5 nozzle. MAP was positioned on the nozzle centreline with adjacent Pitot probes. The overall assembly mounted to a two-axis traverse mechanism, thereby allowing the pitch and yaw to be independently defined. The experimental set up is shown in Figure 11 and a corresponding schlieren photograph (single frame from high speed video) is given in Figure 12. The test results indicated that MAP is capable of resolving increments in alignment of 0.1 degrees which was considered sufficient for the current work and was comparable with similar approaches reported in the literature. The results are report in Bustard (2019) and are to be published at the upcoming 2021 AIAA Aviation Forum and Exposition.

Similar to the total temperature probe, although developed for the current project, MAP has since been used by other experimental programs testing in the High Density Tunnel.

[1] Andrew Bustard is now undertaking a PhD at the University of Notre Dame with Prof. Tom Juliano.

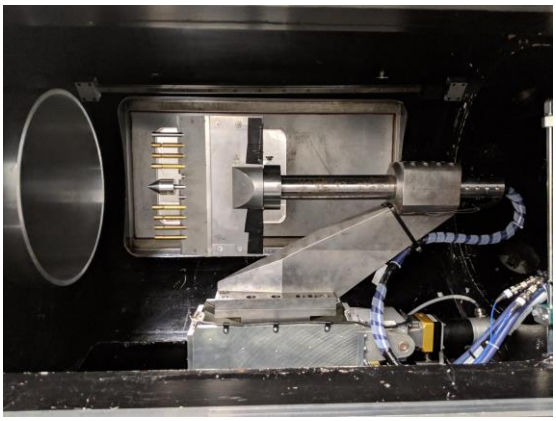

Figure 11: Experimental setup for the evaluation of the Model Alignment Probe at Mach 5. MAP was positioned in the rake on the nozzle centreline. The rake was mounted onto a two-axis traverse.

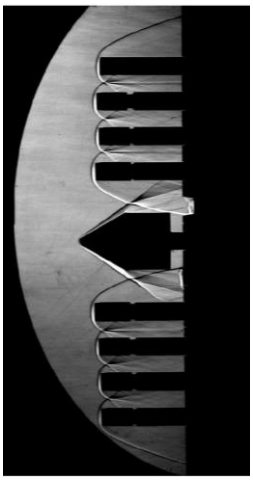

Figure 12: Schlieren photograph of MAP at Mach 5.

2.4 ISO 15377 Calibration Rig

A benchtop calibration rig was developed to enable steady state calibrations of MassCap to be undertaken. Shown in Figure 13, the rig was designed in conformance with BS EN ISO 5167-2:2003. It was connected to a 400 psi supply via a 2-inch regulator which was used to control the supply pressure of the incoming air. The exit of the regulator was connected to a 2 inch 90 deg elbow and a 1100 mm length of 2 inch pipe work. The pipe work was expanded to 4 inch with a concentric expander. A Zanker flow conditioner, designed in accordance with BS EN ISO 5167-2 was installed a distance 1500 mm downstream of the expansion. The conditioner removes large flows distortions in and swirl induced by the elbow, ensuring fully developed pipe-flow upstream of the orifice. A squared-edge orifice plate with diameter 61.2 mm (ratio of 0.6 relative to pipe work internal diameter) was installed 1500 mm downstream of the Zanker flow conditioner. MassCap was installed a further 1500 mm downstream of the orifice and exhausted through a set of silencers.

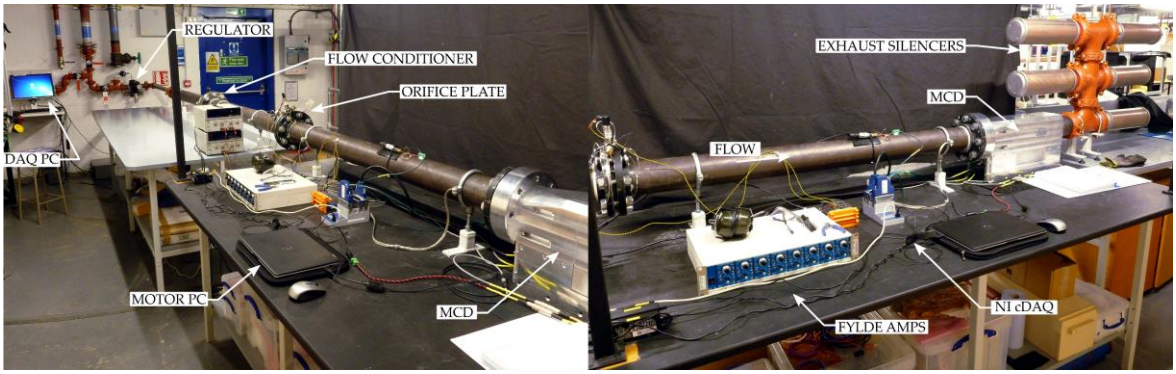

Figure 13: Benchtop Mass Flow Calibration Rig

Instrumentation on the rig included:

- Differential pressure measurement across the orifice (Omega PX419 differential sensor with range 0 to 100 psid and uncertainty 0.08% FS BSL).
- Static pressure upstream of the orifice (Omega PX419 absolute sensor with range 0 to 100 psi and uncertainty 0.05% FS BSL).

- Static pressure 1000 mm downstream of orifice (Sensotechnics CTE gauge-pressure sensor with range 0 to 10 barg and uncertainty 0.1% FS).
- Temperature measurement 1000 mm downstream of orifice (0.005 inch diameter Omega K-type thermocouple positioned within 5 mm of the pipe work centreline).

Overall, the calibration rig produced an uncertainty of just 1.8% for discharge coefficient of MassCap's 40 mm venturi which was considered acceptable for the current work. This uncertainty was dominated by the uncertainties in the differential pressure measurement and the pressure measurement upstream of the venturi. The range of each of these sensors was larger than required, for e.g. the differential pressure was in the range 40 kPa whereas the sensor range was 690 kPa. Replacement of these sensors with similar accuracy, smaller range sensors will reduce the uncertainty in venturi discharge coefficient.

The most significant technical hurdle encountered during benchtop calibrations was achieving choked flow through MassCap's venturi at sufficiently low total mass flow rates. The calibration rig vented to atmosphere through a set of silencers (Figure 13) resulting in a back pressure of ~100 kPa for the venturi. This back pressure is approximately 30 times greater than that achieved in the HDT testing. Consequently, choked flow could not be achieved in the calibration rig for the 60 mm venturi that was used during the first campaign (see campaign summary below) and could only be achieved for the 40 mm venturi used in the second and third campaigns at mass flow rates of in the range 0.8 to 1.2 kg/s. These mass flow rates are 11 to 17 times larger than in the HDT testing with Pitot Intake B (Campaign 2 test condition).

To enable calibrations at lower mass flow rates, the calibration rig must be exhausted into a large vacuum vessel which requires shifting the calibration rig elsewhere in the laboratory. Planning is currently underway for this shift as publication of the campaign 3 results requires updated calibration data.

2.5 Pitot Intakes

Two Pitot intakes were designed and manufactured in this project. These intakes feature 100% capture and were used as calibration intakes for the evaluation of MassCap in the transient test environment of the High Density Tunnel.

Shown in Figure 14, Pitot Intake A featured an inlet diameter of 70 mm and an exit diameter of 60 mm. The inlet diameter was chosen so that the capture area was comparable with the projected capture area of the CREST intake. The contraction ratio of the inlet was 1.17. This small contraction ratio was chosen to ensure that the Pitot intake started. The length of the contracting portion of the inlet was 430 mm and the overall length was 600 mm. Pitot Intake A was instrumented with four Freescale MPXH6400A absolute pressure sensors. These sensors feature integrated amplifiers and have a range 20 kPa to 400 kPa. During the first test campaign however, we found that these sensors are unsuitable for use in the HDT because the lower saturation limit (20 kPa) means that the sensors do not respond to a significant portion of the initial start-up and test flow i.e. the limit is too high for the sensors to be useful.

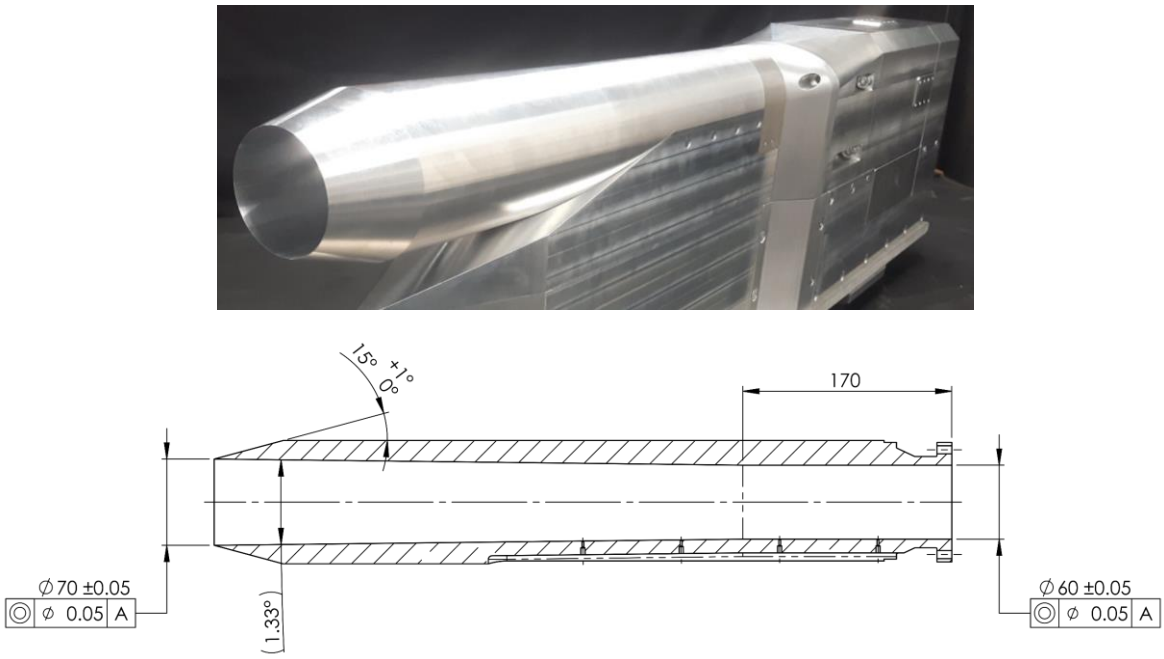

Figure 14: Pitot Intake A. (top) Photograph of Pitot Intake A during dry-assembly. (bottom) Cross-sectional view.

Pitot Intake B is shown in Figure 15. featured an inlet diameter of 36.70 mm and an exit diameter of 31.50 mm with an overall geometric contraction ratio of 1.17. In comparison with Pitot Intake A, this intake was sized so that the exit area is comparable with the exit area of the CREST intake. The length of the contracting portion of the inlet was 297 mm and the overall length was 630 mm. Based on the issues encountered with Pitot Intake A in Campaign 1, Pitot Intake B was instrumented with eight sensors – four Honeywell HSC absolute sensors with range 0 to 15 psi or 0 to 30 psi and four Kulite XTL-140M absolute sensors with ranges either 0 to 70 kPa or 0 to 150 kPa.

The Honewell sensors were observed to operate well during the second test campaign. This work demonstrated that they are a viable alternative to Kulite sensors for experiments that don't require higher bandwidth capabilities of Kulites. Since demonstrating that Honeywell sensors are suitable for use in the HDT, they have been used by a DSTL-sponsored DPhil student as a supplementary measurement.

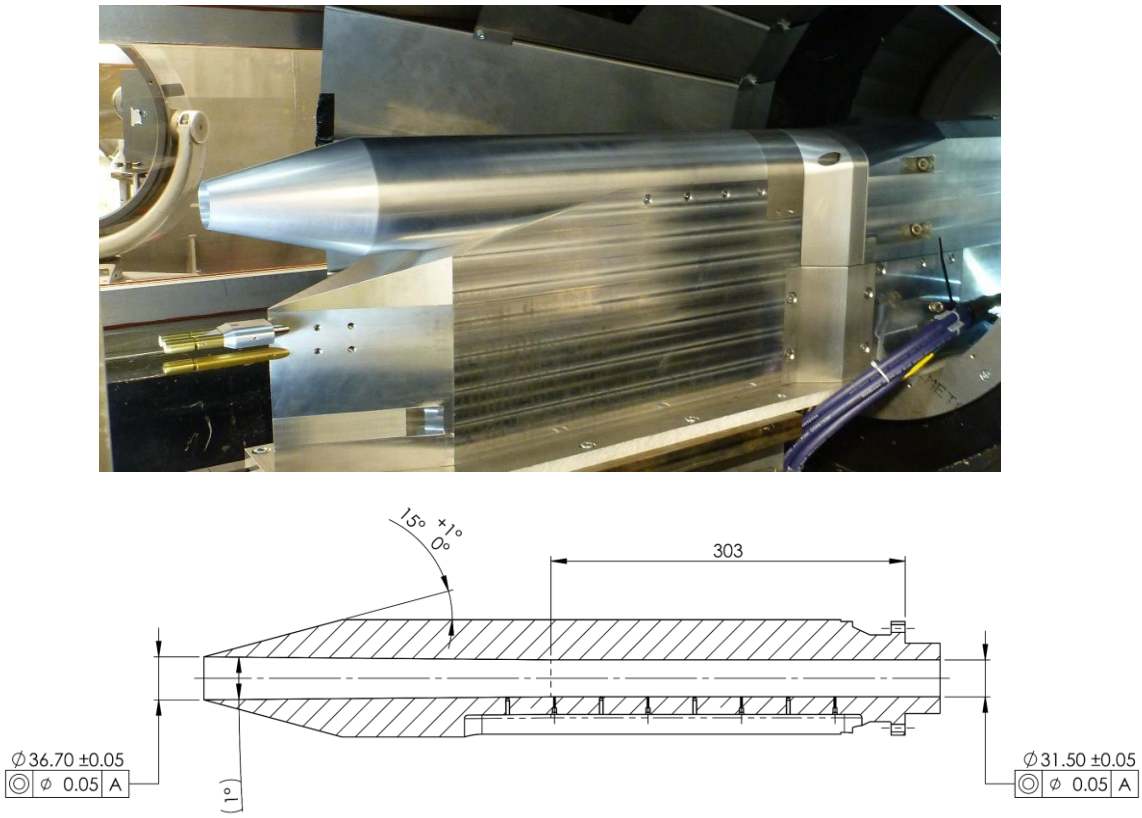

Figure 15: Pitot Intake B. (top) Photograph of Pitot Intake B installed in the HDT test section during Campaign 2. (bottom) Cross-sectional view.

2.6 CREST Intake

The CREST intake developed in this project is shown in Figure 16. The intake underwent a major revision partway through this project. This was completed primarily by UQ who re-developed the internal flow path and major mechanical components. Oxford developed the adaptor which attaches MassCap to the intake. The inlet features a projected capture area of 4,240 mm2 and an exit area of 744 mm2 and has an internal contraction ratio of 1.71. The overall length of the intake was 478 mm and it was mounted to a circular forebody with length 197 mm.

The intake featured 27 pressure ports spaced at 15 mm intervals; 13 were used by the University of Queensland (UQ) during testing in the T4 Shock Tunnel facility. The remaining 14 were used by Oxford for the HDT tests and were instrumented with a combination of Kulite XTL-140M sensors (9-off) and Honeywell HSC sensors (5-off). In the third test campaign in HDT, two additional sensors were added to the forebody. These were used to supplement the Model Alignment Probe for the measurement of yaw angle of the model.

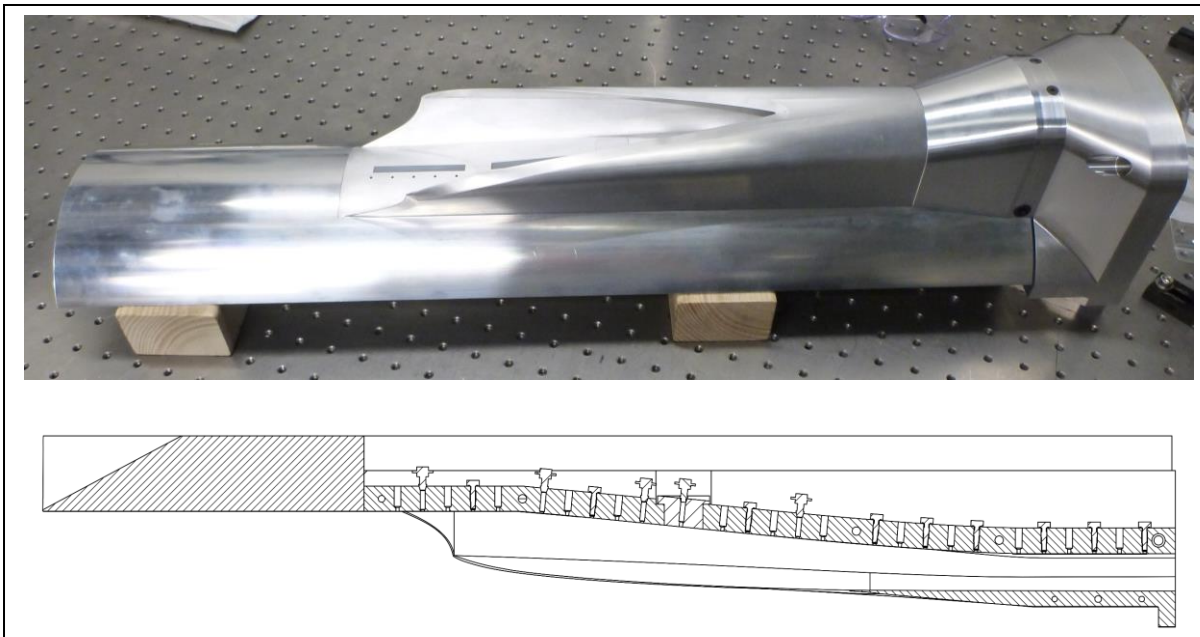

Figure 16: CREST Intake. (top) Photograph prior to installation in the HDT test section. (bottom) Cross-sectional view.

3 Test Campaign Summaries:

This section provides a brief summary of the experimental campaigns that were conducted as a part of this project. The major issues and results obtained in each campaign are highlighted.

3.1 Campaign 1

The first test campaign was conducted in late March 2019 and totalled 12 shots in the HDT. The nozzle exit flow was measured using two pitot pressure probes. Initial tests in this campaign were conducted without the back-pressure device installed such that MassCap was a simply single volume with a venturi at the downstream exit. Both Pitot Intake A and the CREST intake were tested with MassCap in this configuration. Two major technical difficulties were encountered in this campaign:

1. Pitot Intake A did not remain started with a 40 mm venturi fitted in MassCap. This venturi was sized for the CREST intake tests however larger pressure losses through the Pitot intake meant that enough mass could not be driven through the venturi without exceeding the back-pressure capability of Pitot Intake A. This issue was resolved mid-campaign by installing a larger, 60 mm diameter venturi. As discussed in Section 2.4, this venturi was unable to be calibrated on the benchtop rig due to the rig exhausting to atmosphere, restricting our ability to publish the data.
2. The CREST intake appeared to start during flow establishment but un-started at the beginning of the steady flow period. This un-start occurred because the inlet ingested a shock wave originating from the HDT facility nozzle as shown in Figure 17. Altering the axial position of the model with respect to the nozzle exit plane did not change the outcome – within the axial constraints over which the model could be moved, the inlet always swallowed the facility nozzle shock before steady flow was fully established. No useful data was obtained from this campaign for the CREST intake.

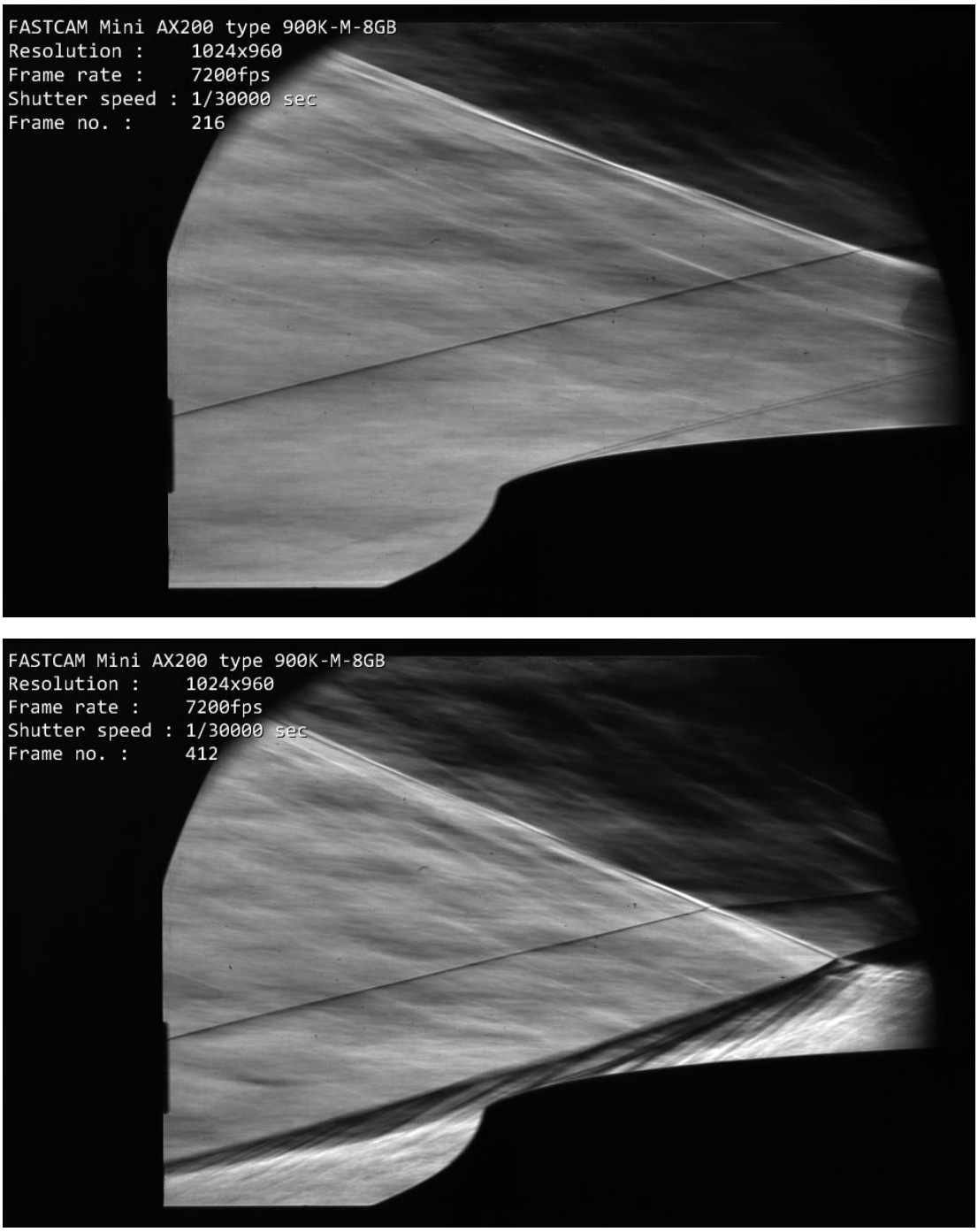

Figure 17: Schlieren images of CREST intake for campaign 1, shot 548. See Figure 20 for a corresponding pressure trace. (top) t = 30 ms after flow arrival. The facility nozzle shock is being swallowed by the intake but has not yet caused a full unstart. (bottom) t = 57 ms after flow arrival. The facility nozzle shock has steepened and the intake is now unstarting.

The presence of the shock wave and its steepening throughout flow onset indicated that the background pressure in the test section was too high (and increasing) causing the facility nozzle flow to collapse. The increasing test section pressure during flow established was hypothesised to be related to the geometry of the HDT test section, which features a large forward-facing step at the exit, and to blockage of the test section exit pipe by the intake-MassCap assembly as shown in Figure 18. During flow establishment there is an increase in mass flow from the facility nozzle which must ultimately exit the test section. The test section geometry and blockage of the model require a higher

test section pressure to drive the required mass flow through the available area at the test section exit, resulting in the facility nozzle flow being over-expanded and the formation of an oblique shock wave. This technical difficulty ultimately resulted in the test campaign being cut short.

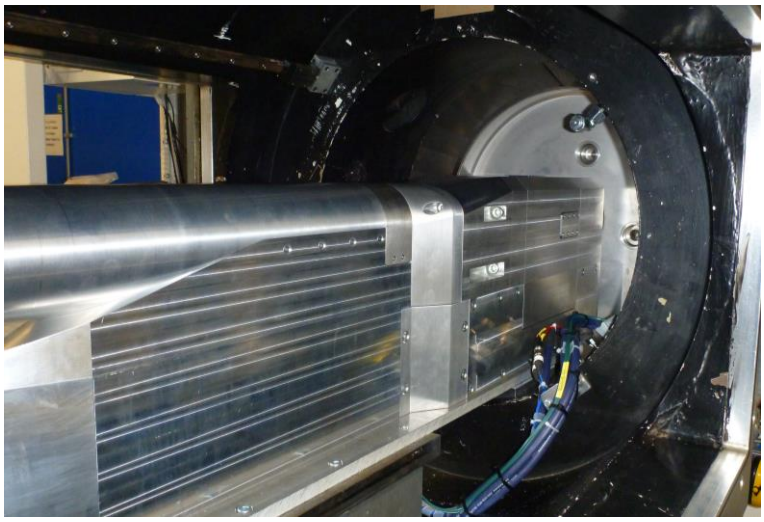

Figure 18: Photograph looking downstream with Pitot Intake A and MassCap installed in the HDT test section. The forward facing step at the exit of the test section is clearly visible as is the size of MassCap relative to the exit pipework.

3.2 Campaign 2

The second test campaign was conducted in September 2019 and totalled 23 shots. The major changes in experimental set up with respect to the first campaign were as follows:

1. Pitot Intake B was used for the in-tunnel calibration tests of MassCap. This intake was designed and built following the first campaign. The smaller capture area meant that it could be used with the nominal 40 mm venturi fitted to MassCap without unstarting.
2. A conical flow deflector, known as the cone-of-shame, was designed and installed by a visiting master's student from the University of Queensland. Shown in Figure 19, this flow deflector was intended to help alleviate adverse effects caused by the forward-facing step at the rear of the test section.
3. A twin-probe mounting was installed and instrumented with two aspirated thermocouples. In combination with a single pitot pressure probe, these were used to monitor the test flow and calculate the freestream mass flux.
4. Freescale pressure sensors used in the intakes were replaced with Honeywell sensors.
5. The mounting hardware was modified to allow the entire assembly to be shifted further upstream than previously possible.

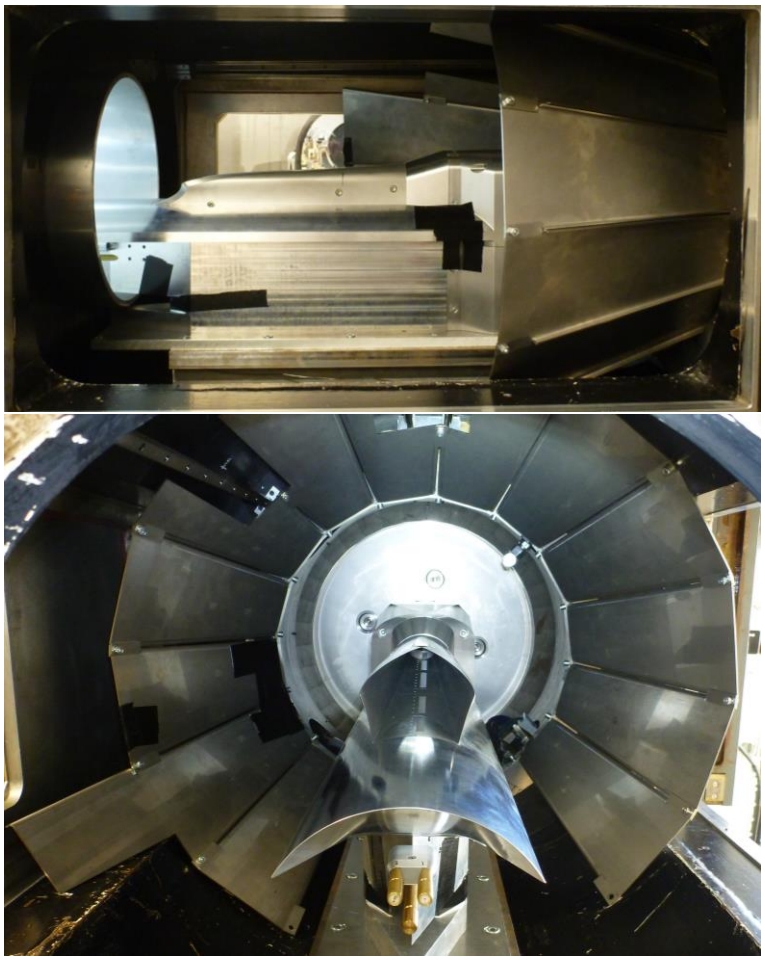

Figure 19: CREST Intake installed in the test section along with the conical flow deflector panels in Campaign 2.

During this campaign, Pitot Intake B was successfully tested with MassCap across a range of different back-pressures where the back-pressure device was held fixed during the test time. The results of these tests, which demonstrated the capability of MassCap in short duration tests, were presented at the 2019 ESA FAR conference. A copy of the paper is included as Appendix A. The difference reported in the paper between the freestream mass flow and that from MassCap was diagnosed in third campaign as being caused by an unknown issue with the pressure sensor located upstream of the venturi. A second sensor was added to this location for the third campaign.

In comparison with Pitot Intake B, tests conducted with the CREST intake were not successful; The adverse interaction with the facility nozzle shock was still present, causing the intake to unstart. Moving the assembly further upstream (relative to positions used in campaign 1) did not significantly delay when the facility wave adversely interacted with the intake. In comparison, installation of the conical flow deflector did slightly delay the onset of the interaction and inlet unstart. This is seen in Figure 20 which plots the nozzle supply pressure traces (K4) and a pressure trace from the rear of the CREST intake (I24) for three test: s548 from campaign 1, s736 from campaign 2, for which the conical flow deflector was installed, and s1094 from campaign 3 for which both the conical flow deflector and a nozzle extension component (aka shark's mouth) were installed (see Section 3.3).

The test condition and model position with respect to the nozzle exit plane were comparable between all three shots. As is clearly seen, inlet unstart was delayed when the conical flow deflector was installed (s548 vs s736) in the second campaign. Despite this improvement, the test time was not

sufficient to fully establish steady flow in the combined inlet-MassCap system. A fully transient analysis is required for this data which has yet to be completed.

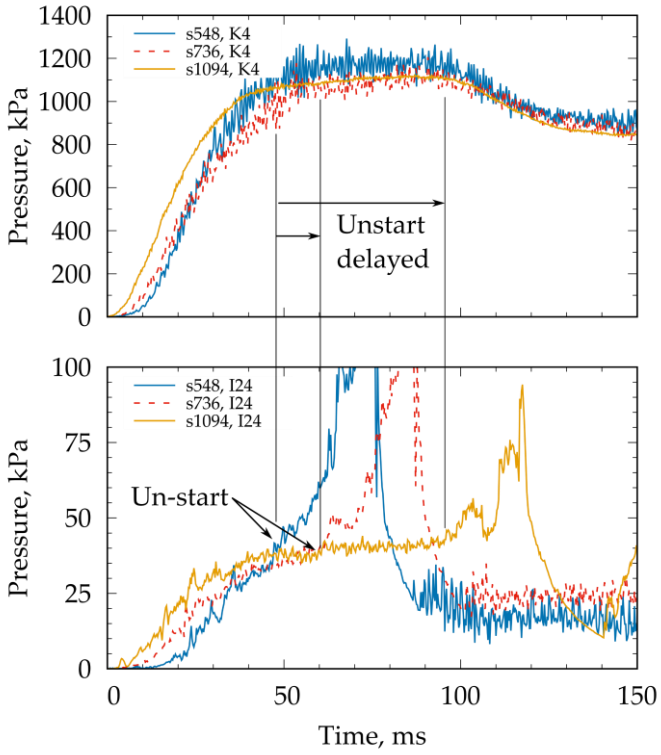

Figure 20: Example pressure traces from Campaign 1 (s548), Campaign 2 (s736) and Campaign 3 (s1094). The upper figure plots the nozzle supply pressure trace (K4). The lower figure plots the trace from the near the end of the CREST intake.

3.3 Campaign 3

The third and final test campaign conducted for this project occurred in August 2020 and totalled 50 shots. The major differences in experimental set up compared with the second campaign were as follows:

1. Additional instrumentation was added to MassCap in the second volume i.e. upstream of the venturi and downstream of the back-pressure device. The new instrumentation consisted of a single Kulite XTL-140 absolute pressure sensor with range 0 to 700 kPa and two 0.003 inch K-type thermocouples. In comparison with the existing thermocouple, which was positioned a few millimetres proud of the internal wall, the two new thermocouples were positioned closer to the centre of MassCap, thus providing an estimate of the thermal gradient that may exist. The lower range of the new sensor (700 kPa compared with 3500 kPa) was expected to significantly improve the overall uncertainty in the calculation of mass flow through the venturi.
2. The model alignment probe developed by Bustard (2019) and described in Section 2.3 was installed in place of the single pitot pressure probe used in the second campaign.
3. An Arduino micro-controller was used to dynamically control the back-pressure device during a test. This system was developed by a visiting UQ master's student, Zaid Nizami as a part of his industry placement at Oxford. He worked at Oxford until the pandemic in early 2020, at which point he returned to Australia and continued to work remotely. Despite significant

effort, dynamic movement of the back-pressure device during the steady test plateau was not fully achieved because we lacked an independent, fast response, measurement of the movement of the dynamic plate. As a consequence, the delay time between the Arduino instructing the motor to move, and the motor actually moving was unable to be quantified, thereby impacting our ability to properly time the motor movement relative to the flow.

4. A flow path extension was developed for the Mach 5 nozzle. Shown in Figure 21, this component is known as the shark's mouth. The idea for this component was originally proposed by Prof. Richard Morgan of the University of Queensland during Prof. McGilvray's doctoral studies. By extending the lip of the nozzle, it was intended that the formation of the nozzle shock would be shifted downstream such that it would interact with the CREST intake downstream of the cowl closure location and would therefore not adversely affect the intake. As shown by the results in Figure 20, the shark's mouth extension had the desired effect, delaying the adverse interaction until the end of the first steady test plateau of the facility.

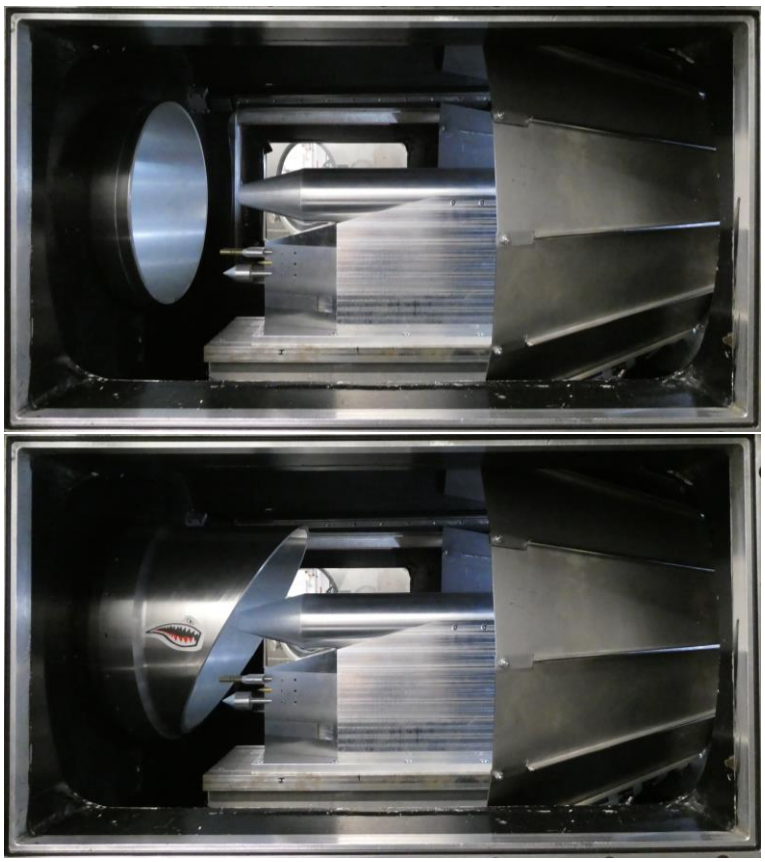

Figure 21: Pitot Intake B installed in the HDT test section during the third test campaign. (top) With the only conical flow deflector installed. (bottom) With both the nozzle extension (shark's mouth) and conical flow deflector installed.

During this campaign, Pitot Intake B was once again successfully tested with MassCap. A range of test conditions and back-pressure device settings were used. The additional instrumentation installed in MassCap upstream of the venturi, confirmed that there was an issue with the pressure measurement Campaign 2. With the new sensors, excellent agreement was achieved between the mass flow calculated from the freestream and that measured by MassCap. The Pitot Intake B tests also confirmed that installation of the shark's mouth extension did not alter the test condition. We intend to update the 2019 FAR paper (given in Appendix A) with data from Campaign 3 and send it out for publication. Re-calibration of MassCap on the benchtop rig is required however to ensure the range of mass flows

over which the calibration is completed is comparable with the mass flows experienced in the HDT tests and that the instrumentation installed in MassCap is consistent.

The combination of the shark's mouth extension and conical flow deflector at the rear of the test section slowed the steepening of the facility nozzle shock such that the interaction with the CREST intake did not occur until near the end of the first steady test plateau of the facility. Although the flow through MassCap was not fully established in this test period and will require transient analysis, this steady flow period was sufficient to examine the back-pressure capability of the CREST intake. Example data are shown in Figure 22 which presents the static pressure distribution through the intake for different settings of the back-pressure device given as the restrictor flow-through area as a percentage of the projected capture area of the intake. It can be seen that the pressure distributions are identical for the cases where MassCap was installed but the back-pressure device was kept fully open (s1094) and where MassCap wasn't installed (s1105). This gives confidence that MassCap does not impart significant back-pressure to the intake when fully open. As the restrictor is close down, a shock-train system is pushed upstream up the inlet.

Further analysis is required to examine the mass capture of the intake. We intend to fully publish this data, including comparison with numerical simulation in the coming year.

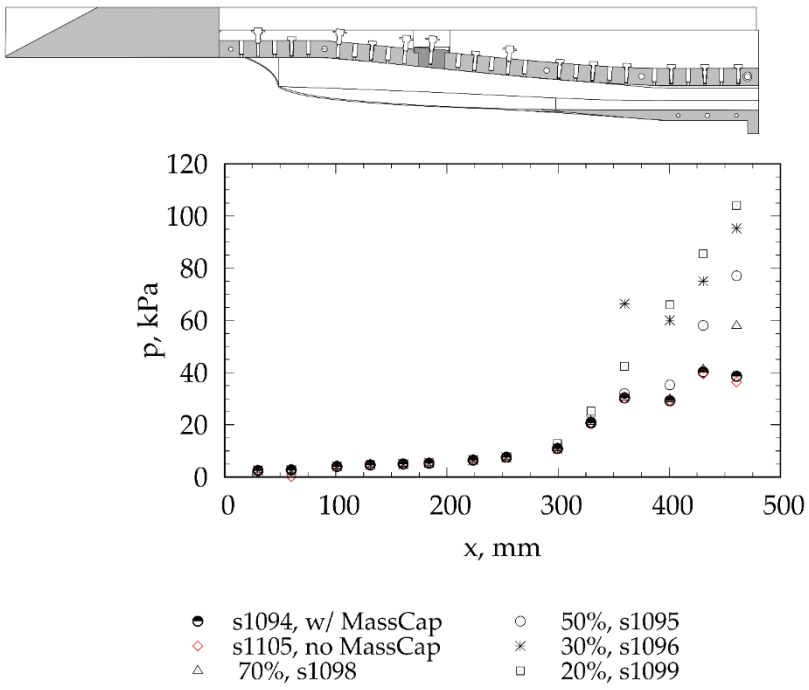

Figure 22: Pressure distribution through CREST intake for different settings of the back-pressure device. Percentages are with respect to the projected inlet capture area.

4 Conclusion and Future Work

This project set out to characterise the mass capture capability of a new generation of shape-transitioning, three-dimensional scramjet intakes using the Oxford High Density Tunnel. Although this goal was not quite achieved, significant technical capability was developed, in particular the novel mass capture device that was developed and validated for short duration test environments. The forward facing step at the exit of the HDT test section, in combination with the large size of the intake

and MassCap assembly, resulted in a collapse of the facility nozzle flow prior to establishment of steady flow. This issue was partially mitigated by the installation of a conical flow deflector at the rear of the test section and an extension piece to the facility nozzle. Ultimately, this interaction adversely affected testing, such that the original project goals were not fully realised. Further work is required and will focus on three key areas:

1. Reducing the blockage created by the intake and MassCap assembly.
2. Developing a new test section for the HDT that removes the forward-facing step at the exit and which improves optical access for advanced diagnostics.
3. Further developing the capability to dynamical move the back-pressure device at speeds relevant for testing in the HDT.

References

Bustard, A (2019) *The Development of a Model-Alignment Probe for the Oxford High Density Tunnel*, B.ASc thesis, University of Toronto, Canada.

Gollan, RJ and Smart, MK (2013) "Design of Modular Shape-Transition Inlets for a Conical Hypersonic Vechicle," *Journal of Propulsion and Power,* vol. 29, no. 4, pg. 832 – 838.

Hermann, T, McGilvray, M, Hambidge, C, Doherty, LJ, and Buttsworth, D (2019) "Total Temperature Measurements in the Oxford High Density Tunnel," in: *International Conference on Flight Vehicles, Aerothermodynamics and Re-entry Missions & Engineering (FAR)*. 30th September – 3rd October, Monopoli, Italy.

Nizami, SZ (2020) *Enhancing diagnostic and testing capability at Oxford Thermofluids Institute*, BEng/MEng Industry Placement Report, University of Queensland, Australia.

Preller, D and Smart, MK (2017) "Reusable Launch of Small Satellites Using Scramjets," *Journal of Spacecraft and Rockets,* vol. 54, no. 6, pg. 1317 – 1329.

Smart, MK (1999) "Design of Three-Dimensional Hypersonic Inlets with Rectangular-to-Elliptical Shape Transition," *Journal of Propulsion and Power*, vol. 15, no. 3, pg. 408 – 416.

Widodo, A and Buttsworth, D (2013) "Stagnation Temperature in a Cold Hypersonic Flow Produced by a Light Free Piston Compression Facility," *Experiments in Fluids*, vol. 54, no. 1486.

Appendix 1: 2019 FAR Paper

The results of Campaign 2 were presented at the 2019 International Conference on Flight Vehicles, Aerothermodynamics and Re-entry Missions & Engineering (FAR). A copy of the paper is included in this appendix. The full citation is as follows:

Doherty, LJ, Hambidge, C, Ivison, W, Hyslop, A, and McGilvray, M (2019) "Development of a Novel Mass Flow Measurement Device for High Speed Inlet Testing," In: *International Conference on Flight Vehicles Aerothermodynamics and Re-entry Mission \& Engineering (FAR)*. 30th September – 3rd October, Monopoli, Italy.

DEVELOPMENT OF A NOVEL MASS FLOW MEASUREMENT DEVICE FOR HIGH SPEED INLET TESTING

Luke J. Doherty, Chris Hambidge, Will Ivison, Andrew Hyslop, Matthew McGilvray

University of Oxford
Oxford Thermofluids Institute
Department of Engineering Sciences
Osney Mead, OX2 0ES, Oxford, UK

Michael K. Smart

University of Queensland
Centre for Hypersonics
School of Mechanical and Mining Engineering
St Lucia, QLD 4072, Australia

ABSTRACT

A novel mass capture device for testing high speed inlets in short duration facilities has been developed. The device improves upon the accuracy and sensitivity of current methodologies by separating the mass flow measurement from the back-pressure inducing capability. It also has sufficient temporal response for reliable application to short duration test facilities. This paper describes the principles of the operation and the design process of the mass capture device. Calibration was performed using a steady flow bench top test using an orifice mass flow meter. The device's suitability for use in transient hypersonic flow facilities was validated in the Oxford High Density Tunnel by connection to a simple Pitot inlet that achieves full mass capture.

Index Terms— Supersonic, Inlet, Mass Capture, Scramjet

1. INTRODUCTION

Air breathing vehicles that fly much faster than the speed of sound, such as ramjets and scramjets, rely solely upon the inlet geometry to perform compression of the incoming freestream air. The amount of mass captured by the inlet is a critical parameter that affects the overall performance and efficiency of the engine. Van Wie [1] predicted that to maintain 1 % accuracy in specific impulse over the range Mach 5 to 10, the accuracy in mass capture must be in the range 1 to 3 %. The ability of an inlet to self-start is also desirable due to the operational simplicity this affords. Both the self-starting and mass capture characteristics are highly sensitive to the flow fields produced by any given inlet geometry, so it is vital that numerical predictions of performance be validated against accurate experimental measurement of these inlet characteristics.

With the prohibitive cost of flight testing, inlet characterisation is typically performed in high speed wind tunnels. Tests are conducted at conditions that match the flight Mach and Reynolds numbers, thereby ensuring similarity of the flow field. Mechanically increasing the back-pressure until the inlet unstarts permits quantification of the effects of combustor operating pressure on the mass capture and the self-starting capability of the inlet.

Shown schematically in Figure 1, a traditional method for high speed inlet mass flow measurement uses a translating cone to restrict the flow exiting from a dump isolator. The mass flow measurement is taken where the gas chokes when passing the cone. This type of device allows some modulation in the annular restriction of the back-pressure to the inlet. Typically, baffle plates and flow straighteners are used to ensure that the measurements of total pressure and total temperature are representative of the stagnated flow. Devices of this sort have been successfully incorporated in testing in the NASA blowdown tunnels by Smart [2] and several tests in the H2k facility [3–6]. In the work described in Hohn and Gülhan [4], an accuracy of ±3 % for the mass flow rate was achieved.

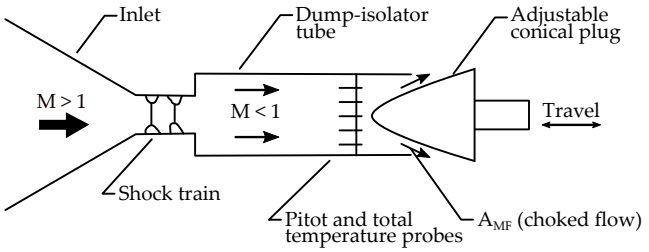

Fig. 1. Schematic of traditional method for inlet mass capture measurement device.

The difficulties with such a device are (1) uncertainties due to the sensitivity and non-linearity of the back-pressure to the position of the rear cone, (2) large response times of the device, specifically the temperature measurement and fill times when tested in short duration facilities, (3) coupling of the back-pressure with the mass flow rate, and (4) the use of non-ISO-standard measurement geometry decreases accuracy over wide ranges of Reynolds numbers.

This paper describes a novel mass capture device where the mass flow measurement and back-pressure functions are separated in order to provide improvements over traditional de-

signs. Section 2.1 describes the principles of operation, design and instrumentation. Steady-state calibration results, in which the device was compared against an ISO 15377 orifice plate, are also presented in Section 2.1, providing accurate characterisation of the device. Section 3 describes the performance for high speed, short duration tests by presenting results of a 100 % capture Pitot inlet that was tested in the Oxford High Density Tunnel (HDT). As a result, the ability of this novel device to accurately characterise the mass capture and back-pressure capability of hypersonic inlets has been demonstrated. The paper finishes in Section 4 with some conclusions and an outlook to future work.

2. NOVEL MASS CAPTURE DEVICE

2.1. Principles of Operation

A new back-pressure/mass flow measurement device was developed which separates the measurement of mass flow from the back-pressure capability. Shown schematically in Figure 2, the device consists of a dump-isolator downstream of the inlet and a secondary isolator downstream of a variable area restrictor. Through careful selection of the area ratios for the combined device-inlet system, which account for the dynamic head losses, the variable area restrictor sets the back-pressure to the inlet while the subsequent subsonic flow downstream is re-accelerated through a fixed area, choked nozzle, providing accurate measurement of the mass flow.

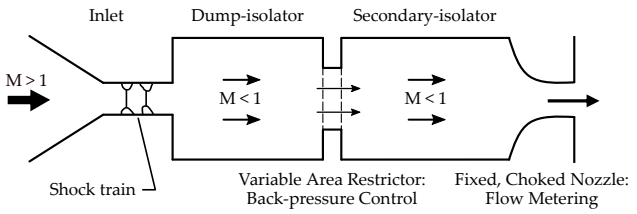

Fig. 2. Schematic of inlet mass capture measurement device with separated back-pressure and mass capture function.

The variable area restrictor consists of two perforated, circular plates that rotate relative to each other in a controlled manner (Figure 3). The upstream plate is held fixed while the downstream plate is rotated by a stepper motor, housed outside the main flow path, via a spur gear mechanism. Since the plate is driven perpendicular to the flow, the motor experiences less load than the translating cone device as shown in Figure 1. Rapid, controlled changes in restriction area are possible, potentially allowing the mass capture characteristics during a complete start-unstart event of an inlet to be recorded transiently in a single experiment. Furthermore, the hole patterns may be specified so as to optimise the back-pressure profile relative to the actuation.

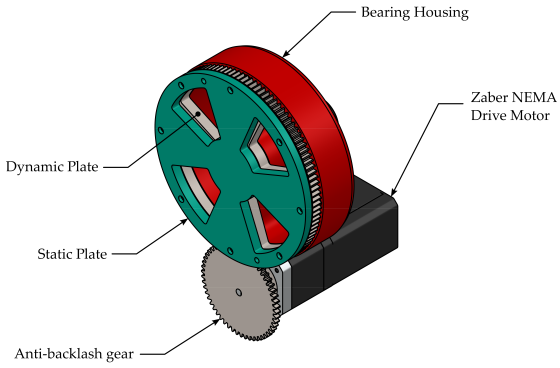

Fig. 3. Isometric view of variable area restrictor and drive motor.

2.2. Design and Instrumentation

The mass capture device (MCD) is shown in Figure 4 together with the Pitot inlet used for validation experiments. Both were machined from 7075-T6 billet aluminium. The MCD features a 120 mm diameter bore that is 410 mm in length and has a maximum pressure rating of 35 bar. The flow exits through a $d_{nt} = 40.00(4)$ mm diameter venturi nozzle that has an internal profile in accordance with ISO 9300:2005(E). The variable area restrictor was located 204 mm downstream of the entrance to the MCD. In the current configuration, both the static and dynamic circular plates featured four circumferential slots as shown in Figure 3. The dynamic plate was manufactured from a Reliance Precision Ltd spur gear (PNo. S1.25S 110A-0818F) and was driven using a Zaber NEMA stepper motor (PNo. X-NMS17CWE01-KX13CG) via. a Reliance Precision Anti-backlash gear (PNo. AP125S1B5F35A-35).

The MCD was instrumented with three Kulite® XT-190(S)M absolute pressure transducers. Labelled P_{MC2}, P_{MC3} and P_{MC4} in Figure 4, each had a range of 0 to 3500 kPa and uncertainty ±0.1 % FS. P_{MC2} and P_{MC3} were located upstream and downstream of the restrictor (respectively) while P_{MC4} was located at the exit of the MCD and, in combination with P_{MC3} on the backward facing step, was used to monitor the pressure ratio across the venturi nozzle. A fourth measurement location, P_{MC1}, was located on the backwards facing step at the entrance to the MCD but was not instrumented in this work.

The temperature upstream of the venturi, T_{MC2}, was measured using a 0.005 inch diameter Omega K-Type thermocouple (PNo. TT-K-36-SLE) housed in a bespoke mounting body. This mounting body positioned the thermocouple bead approximately 1 mm proud of the internal surface. The uncertainty of the thermocouple was 1.1 K.

To enable validation experiments in the Oxford HDT, a Pitot inlet that achieves a 100 % capture ratio of the freestream was designed. It featured an inlet diameter of 36.70(5) mm and an exit diameter of 31.50(5) mm, giving a contraction ratio of 1.17. This small contraction ratio was chosen to ensure that

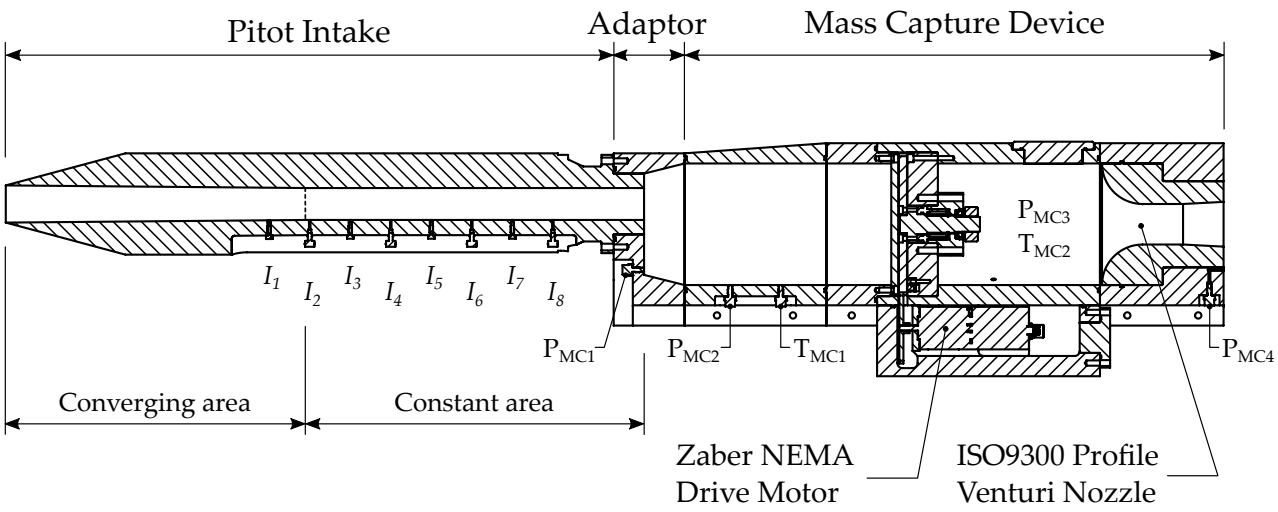

Fig. 4. Cross-section through the mid-plane of the Mass Capture Device. For clarity, the associated mounting hardware is not shown.

the Pitot inlet started. The length of the contracting portion of the inlet was 297 mm and the overall inlet length was 630 mm. The inlet was instrumented with a combination of Kulite® XTL-140M absolute pressure transducers with ranges 0 to 70 kPa (I_1) and 0 to 150 kPa (I_3, I_5, I_7) and Honeywell HSC absolute pressure transducers with ranges 0 to 15 psi (I_2, I_4) and 0 to 30 psi (I_6, I_8). The associated uncertainties are taken to be ±0.1 % FS and ±1 % FS for the Kulite® and Honeywell sensors respectively.

2.3. Benchtop Calibration Rig

A bench top rig was developed to calibrate the MCD under steady flow conditions and to allow examination of the response time of the system. Shown in Figure 5, the rig was designed in accordance with BS EN ISO 5167-2:2003 and featured a 61.2 mm diameter, squared-edged orifice plate (Rototherm PNo. FOP-SM1-100M-01700x0003/125x32/N0.0-562291). The calibration rig was connected to a large reservoir of 400 psi air via a 2 inch IMI Norgren pilot regulator (PNo. R18-B00-RNXD) which was used to control the supply pressure of the incoming air.

The exit of the regulator was connected to a 2 inch 90° elbow and a 1100 mm length of 2 inch pipe work. The pipe work was expanded to 4 inch using a Victaulic No. 50 concentric expander/reducer. A Zanker flow conditioner, designed in accordance with BS EN ISO 5167-2, was installed a distance 1500 mm downstream of the expansion; this distance was 15D relative to the nominal internal diameter of the pipe work. The orifice plate was located a further 1500 mm downstream of the Zanker plate. The MCD was connected 1500 mm downstream of the orifice plate via. a bespoke flange which increased from 102 to 120 mm diameter via. 10.5° half-angle expansion. At the exit of the MCD the air flow was exhausted to atmosphere through four ASCOnumatics high flow mufflers (PNo. SE200HB).

The internal diameter of the pipe work upstream of the orifice plate was measured to be 101.97 mm. This value was an average of 20 micrometer measurements, with four measurements taken at cross-sections 25 mm, 50 mm, 100 mm, 125 mm and 150 mm upstream of the orifice. The diameter ratio of the orifice plate was therefore $\beta = 0.60$.

The differential pressure across the orifice, ΔP, was measured using an Omega PX419-100DDU5V differential pressure sensor with range 0 to 100 psid and uncertainty ±0.08 % FS BSL. The static pressure upstream of the orifice, P_1, was measured using an Omega PX419-100A10V-EH absolute pressure sensor with range 0 to 100 psi and uncertainty ±0.05 % FS BSL. The static pressure sensor was connected to the same upstream pressure taps as the differential pressure sensor.

The static temperature upstream of the orifice was not directly measured but was calculated from the downstream static temperature, T_3, assuming an isenthalpic expansion (as per the standard). The downstream temperature was measured at a location 1000 mm from the orifice plate using a 0.005 inch diameter Omega K-Type thermocouple (PNo. TT-K-36-SLE). This thermocouple was mounted using 1 mm diameter Scanivalve tube glued into the pipe side wall. The thermocouple bead was ≈5 mm from the pipe centreline. Finally, the downstream wall static pressure, P_3, was measured in the same cross-section as T_3 using a Sensortechnics CTE9010GP0 gauge-pressure sensor with range 0 to 10 barg and uncertainty ±0.1 % FS.

The data acquisition system for the calibration rig consisted of a National Instruments cDAQ-9184 chassis fitted with an NI-9220 analogue voltage input card and the combination of an NI-9214 thermocouple module with TB-9214 isothermal terminal block. Kulite® pressure sensors installed in the MCD were amplified using Fylde FE-H379-TA amplifiers. The calibration

rig and MCD pressure signals were recorded with a sampling rate of 1000 Hz while thermocouple signals were recorded using "high-resolution mode" with a sampling rate of 30 Hz.

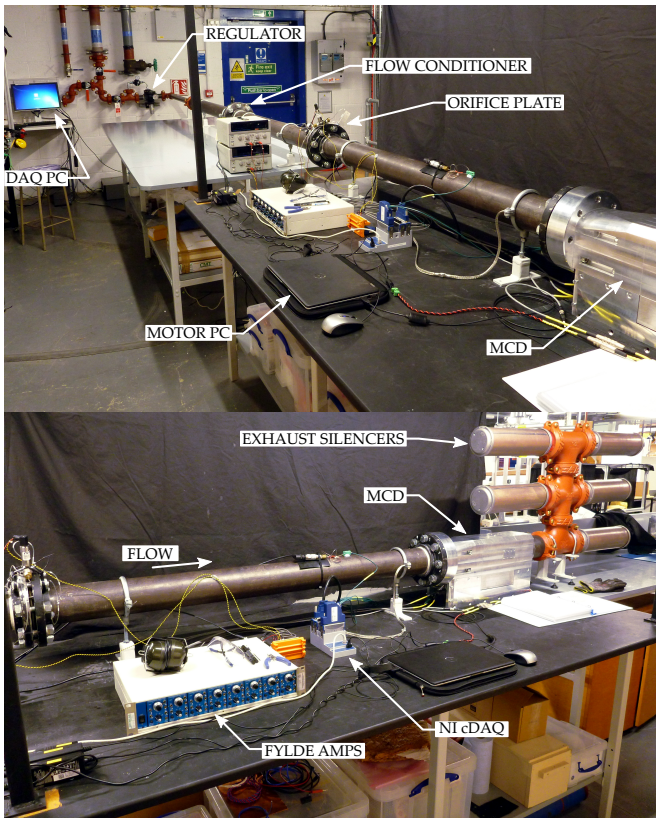

Fig. 5. BS EN ISO 5167-2 Mass-flow Calibration Rig

2.4. Benchtop Calibration Results

Sample transient results obtained from the calibration rig for calibration H are presented in Figure 6. In this calibration, the feed pressure was increased in increments of approximately 100 kPa by (manually) adjusting the upstream pressure regulator (Figure 5). At each increment, the feed pressure was held constant for approximately 10 s to allow the system to stabilise. Each steady plateau in Figure 6 represents one usable calibration interval.

BS EN ISO 5167-2 for the orifice plate and ISO 9300 for the venturi each give criteria on valid ranges for the pressure ratio across each device and the corresponding Reynolds number.[1] In Figure 6, the pressure ratios of the devices are plotted only for their individual ranges of validity; Reynolds numbers and mass flow rates are plotted for the period where the Reynolds number is additionally valid. Finally, the calculated discharge coefficient of the venturi is plotted only where mass flow of both devices is valid.

[1]For the orifice, the Reynolds number is calculated with respect to the upstream flow, $Re_D = 4q_o/(\pi\mu_1 D)$; for the venturi, it is calculated with respect to the throat, $Re_{nt} = 4q_v/(\pi\mu_{MC3}d_{nt})$.

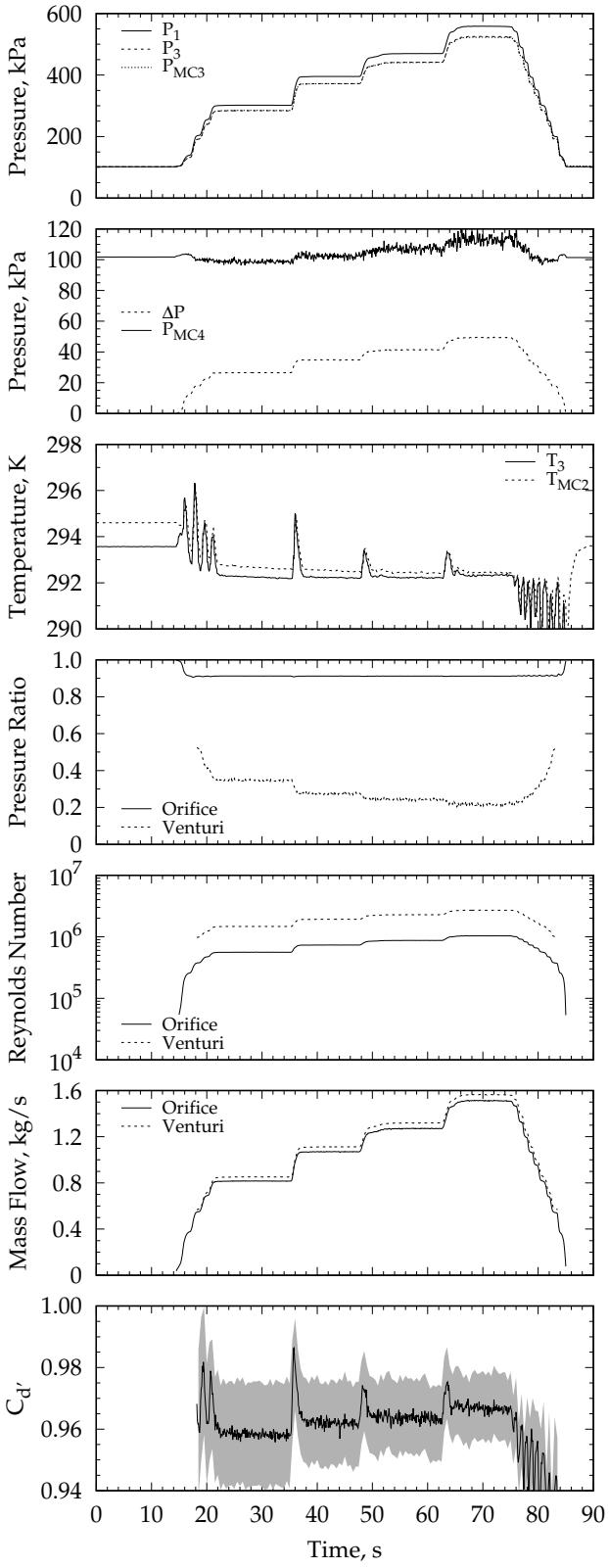

Fig. 6. Time histories recorded for calibration H. All signals have been filtered using a 100 ms moving average filter. The shaded region $C_{d'}$ indicates the experimental uncertainty.

As per BS EN ISO 5167-2, the mass flow through the orifice was calculated using

$$q_o = \frac{C}{\sqrt{1-\beta^4}}\epsilon\frac{\pi}{4}d^2\sqrt{2\rho_1\Delta P} \tag{1}$$

where $C = f(\beta, Re_D)$ is the orifice discharge coefficient, ρ_1 is the static density upstream of the orifice plate, ΔP is the pressure drop across the orifice and ϵ is the expansibility factor given by

$$\epsilon = 1-(0.351+0.256\beta^4+0.93\beta^8)\left[1-\left(\frac{P_1-\Delta P}{P_1}\right)^{1/\gamma}\right] \tag{2}$$

The upstream density ρ_1 was not measured directly in this work but was inferred from the far-downstream temperature and pressure using

$$\rho_1 = \frac{P_1}{R(T_3+\mu_{JT}(P_1-P_3))} \tag{3}$$

where $\mu_{JT} = 0.22\times10^{-5}\,\mathrm{K/Pa}$ is the Joule-Thomson coefficient for air.

For the venturi in the MCD, the mass flow was calculated in accordance with ISO 9300 using

$$q_v' = \frac{A_{nt}C_*P_{0,MC3}}{\sqrt{RT_{0,MC2}}} \tag{4}$$

where A_{nt} is the throat area of the venturi, and C_* is the critical flow function –

$$C_* = \sum_i a_i\left(\frac{P_{0,MC3}}{P_c}\right)^{b_i}\left(\frac{T_{0,MC2}}{T_c}\right)^{c_i} \tag{5}$$

where $P_c = 3.786\,\mathrm{MPa}$ and $T_c = 132.5306\,\mathrm{K}$ are the critical pressure and temperature of air, and $P_{0,MC3}$ and $T_{0,MC}$ are the total pressure and temperature upstream of the venturi which are related to the measured P_{MC3} and T_{MC2} via isentropic flow equations.

Finally, the calibrated discharge coefficient for the venturi was calculated using

$$C_{d'} = \frac{q_o}{q_v'} \tag{6}$$

The uncertainty in the average discharge coefficient from a period in each calibration run was calculated using

$$\begin{aligned} X_{C_{d'}}^2 = {} & X_C^2 + X_\epsilon^2 + \left(\frac{2\beta^4}{1-\beta^4}\right)^2 X_D^2 \\ & + \left(\frac{2}{1-\beta^4}\right)^2 X_d^2 + \frac{1}{4}X_{\Delta P}^2 + \frac{1}{4}X_{\rho_1}^2 \\ & + 2X_{d_{nt}}^2 + X_{C_*}^2 + X_{P_{MC3}}^2 + \frac{1}{4}X_{T_{MC2}}^2 \end{aligned} \tag{7}$$

where $X_a = \frac{\delta a}{a}$ is the relative uncertainty in variable a. The uncertainty in the expansibility factor and upstream density are respectively given by Equations (8) and (9) as follows –

$$X_\epsilon^2 = \left(3.5\frac{\Delta P}{\gamma P_1}\right)^2 \tag{8}$$

$$X_{\rho_1}^2 = \frac{(T_3-\mu_{JT}P_3)^2X_{P_1}^2 + (\delta T_3)^2 + (\mu_{JT}\delta P_3)^2}{\left(T_3+\mu_{JT}(P_1-P_3)\right)^2} \tag{9}$$

Figure 7 plots the averaged discharge coefficient from each calibration interval against the throat Reynolds number, Re_{nt} of the venturi. For clarity, experimental uncertainties are provided for selected calibrations only. Calibrations A, B, C, D and H were each conducted with the restrictor fully open. The flow through area was equivalent to a diameter of 78.7 mm. Calibrations E, F and G were conducted with the restrictor partially closed, with flow-through areas equivalent to diameters of 50 mm, 40 mm and 30 mm, respectively.

The overall average discharge coefficient across all calibrations was $\overline{C}_{d'} = 0.942(17)$ which is indicated in Figure 7 by a horizontal dashed line. Its uncertainty is indicated by the shaded region and accounts for correlated uncertainties between each calibration used in determination of the average.

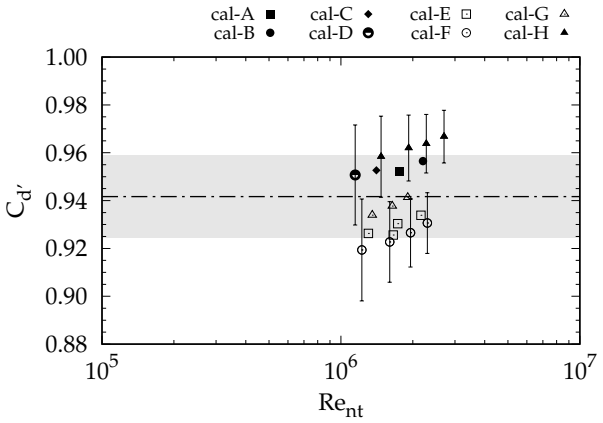

Fig. 7. Discharge coefficient variation with venturi-throat Reynolds number. For clarity experimental uncertainties are provided only for selected calibrations.

The uncertainty in $\overline{C}_{d'}$ corresponds to 1.8 % which was considered acceptable for this initial investigatory work. This uncertainty was dominated by the differential pressure ΔP and venturi static pressure P_{MC3} measurements. Changing the associated sensors would reduce the coefficient uncertainty to approximately 0.5 %.

Figure 7 indicates a slight dependency of the discharge coefficient on the throat Reynolds number, with calibrations performed at higher values of Re_{nt} i.e. higher mass flow rates, having higher discharge coefficients. There also appears to be a small dependency of the discharge coefficient on the status

of the upstream restrictor, with calibrations conducted with the restrictor fully open (filled symbols) resulting in higher discharge coefficients than those conducted with the restrictor partially closed (open symbols). It is expected that these observed dependencies are related to flow non-uniformities within the MCD and the location/measurement of P_{MC3} and T_{MC2}. These sensors could not be located strictly in accordance with ISO 9300 due to size restrictions placed on the MCD by the HDT Test Section and test flow duration. For this work, the dependicies were considered sufficiently small and the overall average $\overline{C}_{d'}$ was taken to be a constant when analysing the HDT data presented in the next section. The flow non-uniformity within the MCD and its influence on the measurement of P_{MC3} and T_{MC2} will be the investigated in future work.

3. EXPERIMENTAL FACILITY AND RESULTS

Experiments to validate the MCD in a short duration test facility were carried out in the University of Oxford's High Density Tunnel. This facility was originally developed by the RAE (later Qinetiq) in the United Kingdom in the 1960's. Constructed from 6-inch gun barrels, the facility was initially operated as a cold hydrogen driven shock tube and tunnel. The HDT, shown on the right in Figure 8, was acquired from Qinetiq in 2012 by the University of Oxford to widen the portfolio of hypersonic ground-test facilities within the Oxford Thermofluids Institute [7]. The facility has been installed and is now fully operational in Ludwieg Tube mode. Futher details of its performance during commissioning are presented in Wylie et al. [8]. This facility is capable of generating relatively long duration flows at high Reynolds number, and is suitable for both steady and unsteady aerothermodynamic testing of hypersonic configurations.

Fig. 8. Hypersonics Laboratory at the Oxford Thermofluids Institute. The T6 Stalker Tunnel is on the left and the High Density Tunnel is on the right.

3.1. Test Conditions

The test flow properties were calculated using the measured nozzle supply pressure (p_0), pitot pressure (p_p) and total temperature (T_0) assuming isentropic flow of calorically perfect air with Keyes model used for the calculation of viscosity.

The facility nozzle supply pressure was measured using a Kulite XT-190(S)M absolute pressure transducer with range 0 to 3500 kPa and accuracy ±0.1 % FS. Additionally, the experimental model was instrumented with a pitot probe and a total temperature probe. The pitot probe was instrumented with a flush-mounted Kulite XCEL-152 absolute pressure transducer with range 0 to 172 kPa and accuracy ±0.1 % FS.

The total temperature probe was based on the work of Widodo and Buttsworth [9] and Hermann et al. [10]. It consisted of a heated aspirated thermocouple housed within a diameter 10.5 mm body and featuring a diameter 1.6 mm through hole. A K-type thermocouple with nominal diameter 0.001 inch was used and the effective length and heat transfer coefficient were characterised to be 1.39 mm and 1114 W/(m^2 K) respectively. Based on the work of Hermann et al. [10] the uncertainty in the total temperature measurement was taken to be ±15 K.

A nominal condition of Mach 5, unit Reynolds number of 14×10^6/m and total temperature of 450 K was used during testing in the HDT. The average test condition across all shots conducted for this work is reported in Table 1.

Table 1. Average Test Condition

p_0	kPa	937	$\pm$ 4
p_p	kPa	60.0	$\pm$ 0.5
T_0	K	449	$\pm$ 15
M		4.95	$\pm$ 0.01
p	Pa	1875	$\pm$ 24
T	K	76	$\pm$ 3
u_x	m/s	866	$\pm$ 15
Re_u	10^6/m	13.6	$\pm$ 0.7
ρu_x	kg/(s m^2)	74.3	$\pm$ 1.4

3.2. Experimental Setup of the Pitot Inlet

The Pitot inlet and MCD assembly is shown installed in the HDT test section in Figure 9. The assembly was positioned such that leading edge of the inlet was 98.0(5) mm downstream of the nozzle exit plane and the inlet centreline was, to within measurement uncertainty, concentric with the nozzle. Previous nozzle survey data indicated that the core flow size of the Mach 5 nozzle was ⌀280(5) mm at 137(5) mm downstream of the nozzle exit plane. The inlet capture area was therefore well positioned within the nozzle core flow.

3.3. Pitot Inlet Results

A set of shots were conducted in the HDT. For each shot, the variable area restrictor (Figure 3) within the MCD was adjusted to a fixed value throughout the duration of test flow. With the variable area restrictor fully open, the flow-through

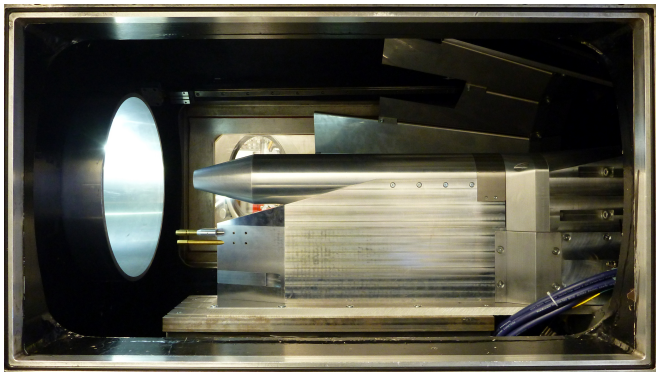

Fig. 9. Pitot inlet installed in the HDT test section with Mach 5 nozzle.

area (A_R) was equivalent to 438 % of the capture area (A_I). Six other settings of the restrictor were tested, corresponding to flow-through area ratios of 110 %, 90 %, 70 %, 50 %, 30 % and 10 %. The measured pressure distribution for each test is presented in Figure 10. Each data point represents the average over the test time of the corresponding sensor. The error bars plotted represent one standard deviation of the variation of each pressure measurement during the test time. A cross-sectional view of the inlet at the correct relative scale is also provided to aid interpretation

For the fully open test ($A_R/A_I = 438\,\%$, shot 716) the pressure distribution is constant and low, representing a fully started inlet. A small pressure increase occurs from I_3 (5.0 kPa) to I_8 (5.7 kPa) due to boundary layer growth. The overall static pressure ratio across the inlet ($I_8/p = 3$) is small, indicating that the freestream is only weakly compressed, as expected for this low contraction ratio design.

When the restrictor is closed, the flow field within the inlet changes such that significantly higher pressures are measured at the rear of the inlet compared with the fully open test. The start of the pressure-rise moves upstream as the flow-through area of MCD decreases. Its shape, a gradual increase in pressure, is indicative of an oblique shock-train [11] being located in the constant area section of the inlet. This shock train features greater levels of unsteadiness compared with the upstream flow, as evidenced by the larger error bars for sensors at the start of the pressure-rise. For restrictor area ratios between 30 % and 110 %, the shock train is contained completely within the inlet, with sensors I_2 to I_4 measuring identical to the fully open test.

In comparison, when the restrictor was set to 10 % of the inlet area, the pressure distribution changed significantly with every sensor elevated to an average pressure level of 54.5 kPa. This average is comparable with the expected post-normal shock pressure of 53.3 kPa calculated using the conditions reported in Table 1. Thus, for this setting of the restrictor, the inlet was unstarted with a bow-shock positioned upstream of the inlet capture area. Thus, the full range of behaviour of the inlet has been induced in a controlled manner, whilst maintaining a fixed mass flow measurement geometry.

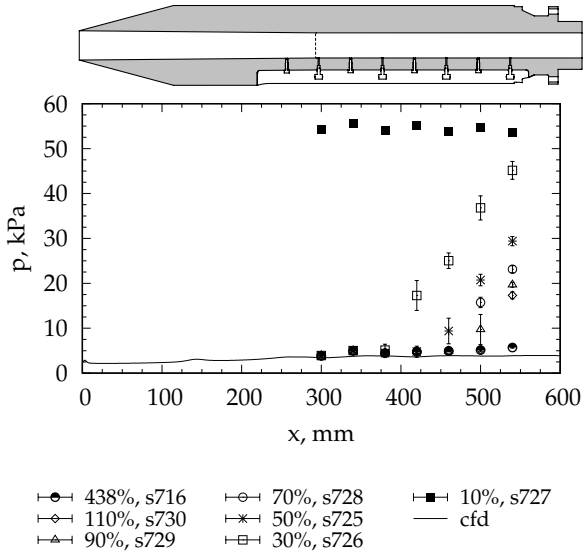

Fig. 10. Experimental static pressure distribution for different settings of the restrictor. Percentages are with respect to inlet capture area (A_I). Error bars represent one standard deviation of the variation during the test time.

Figure 11 presents the variation in inlet back-pressure (P_{MC2}) and mass flow ($q_v = q'_v C_{d'}$; cf. Equations (4) and (6)) with the restrictor area ratio. The freestream mass flow, calculated from the mass flux listed in Table 1 and inlet capture geometry, is indicated by a horizontal dashed line.

As expected, the back-pressure increases as the restrictor is closed, changing from 30 kPa with the restrictor fully open to 62 kPa with the restrictor set at 30 %. A further reduction of the restrictor flow-through area (to 10 %) causes the inlet to unstart and the back-pressure to drop. This lower back-pressure is a consequence of total pressure losses across the bow-shock sitting in front of the inlet. Although the back-pressure was lower than when the restrictor was set to 30 %, the inlet remained un-started throughout the test flow duration.

The measured mass flows presented in Figure 11 show no variation with the restrictor area ratio provided the inlet is started. This result demonstrates that the venturi mass flow measurement capability is independent of the back-pressure capability, proving the overall design of the MCD.

The average mass flow for the started inlet was measured to be 69(9) g/s, compared with 79(2) g/s calculated from the freestream mass flux and inlet capture area. This is just within the uncertainty of the MCD mass flow (approximately 13 %) which was dominated by $X_{P_{MC3}}$ and so is easily reduced in future tests by a change in pressure transducer.[2]

[2]For example, changing P_{MC3} to a transducer with range 150 kPa and uncertainty ±0.1 % FS reduces the mass flow uncertainty to approximately 2 % (excluding corresponding improvements in $X_{\overline{C}_{d'}}$)

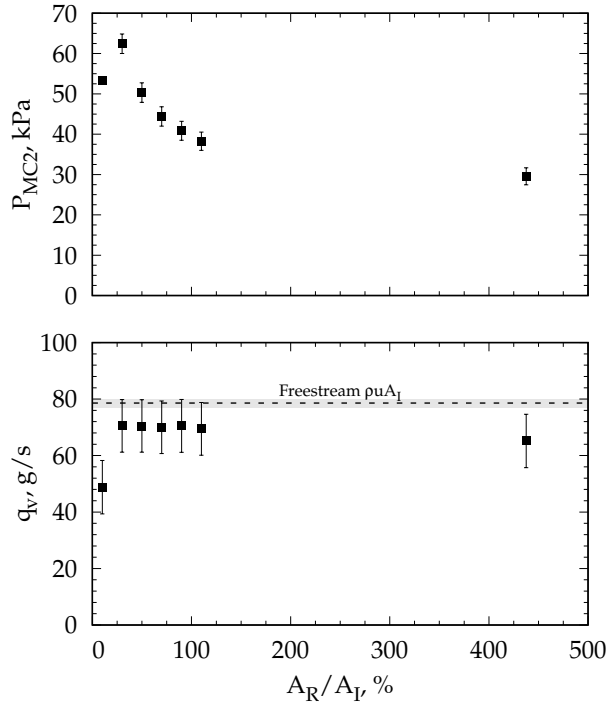

Fig. 11. Variation in back-pressure (P_{MC2}) and measured mass flow (q_v) with restrictor area. The restrictor area is given as a percentage of the capture area of the Pitot inlet. Error bars for the back-pressure represent one standard deviation of the variation during the test time; error bars for the mass flow represent the systematic experimental uncertainty.

4. CONCLUSION

This work presents the development of a novel mass capture device capable of accurate measurement of mass flow rates in short duration test facilities. The new device separates the mass flow measurement capability from the back-pressure inducing capability, improving the overall versatility. The device was calibrated against an orifice plate using a new steady-flow bench top test rig. A calibration uncertainty of 1.8 % was achieved, with scope for this to be reduced to 0.5 %. Short-duration validation experiments were carried out in the High Density Tunnel at a Mach 5 test condition with a simple Pitot inlet and demonstrated the devices operating capability. In future work, this novel device will be used to characterise the mass capture and back-pressure capability of a flight-representative scramjet inlet.

ACKNOWLEDGEMENTS

The authors would like to thank the efforts of Professor Russ Cummings in help defining the work. We would also like to thank Dr Chris Owen (Tata Steel Europe) and Steve Pickett (CMT Engineering) for supplying the calibration rig piping, Greg King for instrumenting the total temperature probe and creating the Honeywell sensor circuit boards, and Tobias Hermann for operating the HDT. This work was funded under EOARD grant FA9550-18-1-0022.

REFERENCES

[1] D. Van Wie, "Scramjet Inlets," in *Scramjet Propulsion*, ser. Progress in Astronautics and Aeronautics, E. T. Curran and S. N. B. Murthy, Eds. Washington, DC.: AIAA, 2000, vol. 189, pp. 447–511.

[2] M. K. Smart, "Experimental Testing of a Hypersonic Inlet with Rectangular-to-Elliptical Shape Transition," *Journal of Propulsion and Power*, vol. 17, no. 2, pp. 276 – 283, 2001.

[3] J. Häberle and A. Gülhan, "Investigation of the Performance of a Scramjet Inlet at Mach 6 with Boundary Layer Bleed," in *14th AIAA/AHI Space Planes and Hypersonics Systems and Technologies Conference*, no. AIAA-2006-8139, Canberra, Australia, 06 – 09 November 2006.

[4] O. M. Hohn and A. Gülhan, "Experimental Investigation of Sidewall Compression and Internal Contraction in a Scramjet Inlet," *Journal of Propulsion and Power*, vol. 33, no. 2, pp. 501–513, March 2017.

[5] A. Flock and A. Gülhan, "Experimental and Numerical Performance Analysis of a Self-Starting Three-Dimensional Scramjet Intake," *Journal of Propulsion and Power*, vol. 33, no. 6, pp. 1570 – 1580, Nov. 2017.

[6] J. Steelant, R. Varvill, S. Defoort, K. Hannemann, and M. Marini, "Achievements Obtained for Sustained Hypersonic Flight within the LAPCAT-II Project," in *20th AIAA International Space Planes and Hypersonic Systems and Technologies Conference*, no. AIAA-2015-3677, Glasgow, Scotland, 06 – 09 July 2015.

[7] M. McGilvray, L. J. Doherty, A. J. Neely, P. T. Ireland, and R. Pearce, "The Oxford High Density Tunnel," in *20th AIAA International Space Planes and Hypersonic Systems and Technologies Conference*, no. AIAA-2015-3548, Glasgow, Scotland, 06 – 07 July 2015.

[8] S. Wylie, L. J. Doherty, and M. McGilvray, "Commissioning of the Oxford High Density Tunnel for Boundary Layer Stability Measurements at Mach 7," in *48th AIAA Fluid Dynamics Conference*, no. AIAA-2018-3074, Atlanta, Georgia, United States, 25 – 29 June 2018.

[9] A. Widodo and D. Buttsworth, "Stagnation Temperature in a Cold Hypersonic Flow Produced by a Light Free Piston Compression Facility," *Experiments in Fluids*, vol. 54, no. 1486, Mar. 2013.

[10] T. Hermann, M. McGilvray, C. Hambidge, L. Doherty, and D. Buttsworth, "Total Temperature Measurements in the Oxford High Density Tunnel," in *International Conference on Flight Vehicles, Aerothermodynamcis and Re-entry Missions & Engineering (FAR)*. Manopoli, Italy: ESA, 30 September – 3 October 2019.

[11] F. S. Billig, S. Corda, and P. P. Pandolfini, "Design Techniques for Dual Mode Ram-Scramjet Combustors," in *Propulsion and Energetics Panel, 75th Symposium*, ser. AGARD Conference Proceedings, vol. 479, 1990.